THE PENNSYLVANIA STATE UNIVERSITY
SCHREYER HONORS COLLEGE

DEPARTMENT OF MECHANICAL AND NUCLEAR ENGINEERING

EFFECTS OF DILUTION JET PLACEMENT AND RESULTING COHERENT STRUCTURES ON TURBINE FLOW FIELDS AND HEAT TRANSFER

ENRICO B. DELLA CORNA
SPRING 2015

A thesis
submitted in partial fulfillment
of the requirements
for a baccalaureate degree
in Mechanical Engineering
with honors in Mechanical Engineering

Reviewed and approved* by the following:

Stephen Lynch
Assistant Professor of Mechanical Engineering
Thesis Supervisor

Hosam Fathy
Assistant Professor of Mechanical Engineering
Honors Adviser

* Signatures are on file in the Schreyer Honors College.

ABSTRACT

A key to increasing performance of high power gas turbine engines is improved understanding of crucial components such as the combustion chamber and first vane cascade. While these systems provide a significant portion of the engine's power, there are many intricacies to their interactions which are not fully understood.

Dilution jets are introduced to the combustion chamber to help create uniform exit flow and aid fuel-air mixing. However, unsteady flow structures result from these jets entering the crossflow and lead to uneven velocity and temperature profiles at the combustor exit. A large body of prior work exists which characterizes flow within the combustion chamber both experimentally and computationally. This is also true of work regarding flow and heat transfer at the turbine first vane. Less research exists that focuses on the interaction between the large-scale structures created by dilution jets and their direct impact on the first vane.

This work created computational models of a standard combustor setup as well as two similar configurations that varied the placement of the dilution jets in relation to the first vane. A steady RANS model was used to simulate turbulent flow through each setup.

The resulting models determined that dilution jet placement could influence heat transfer levels on the first vane. Decreasing the stream-wise distance between the dilution holes and the first vane created large velocity gradients at the turbine inlet, and subsequently produced highly varied heat transfer at different regions along the first vane. Shifting the holes to create alignment of the second row of jets and the vane leading edge appears to induce lower and more even heat transfer on the vane surface, calling for further investigation of this design.

TABLE OF CONTENTS

NOMENCLATURE

C	=	mixing effectiveness (from Eq. 1, Holdeman mixing parameter)
H	=	height of duct at injection plane (from Eq. 1)
h	=	heat transfer coefficient, $h = q/\Delta T$ in W/(m^{2}K)
J	=	momentum flux ratio between jet and freestream
J_f	=	forward dilution momentum flux ratio
J_r	=	rear dilution momentum flux ratio
q	=	heat flux, $q = dQ/dA$ in W/m^2 where Q is thermal power
S	=	spacing between orifice mid-points (from Eq. 1)
T_∞	=	freestream temperature
T_c	=	coolant temperature
U_∞	=	main inlet velocity

LIST OF FIGURES

LIST OF TABLES

ACKNOWLEDGEMENTS

First and foremost, I would like to thank Dr. Lynch for all of his help and guidance throughout this entire process. Not only have your lightning-fast email responses made it easy to work with you, but your great teaching ability and easy-going nature have made writing this thesis an enjoyable and extremely educational experience. I also want to thank Mike and all the other students in the lab who were always willing to lend me a hand or commiserate about computer issues, I might still be trying to set up my Pointwise grid if it weren't for your help. Last, but certainly not least, thanks to all of my family and friends, not only for your love and support through this process, but throughout my college career and beyond. I can't imagine where I'd be without all of you.

Chapter 1

Introduction

Gas turbine engines have a variety of purposes in modern industry and society, from industrial power generation to powering cutting edge fighter jets. These engines have found their way into numerous types of vehicles, however the high power-to-weight ratio that they boast works particularly well in marine and flight applications. The motivation for this thesis is improving the performance of gas turbines for jet engine applications.

Ever increasing demands for the performance of gas turbine engines have driven vast improvements over the past 60 years, in which the thrust capabilities of these engines has increased from around 5 to 155 kilonewtons, and in turn have led to speeds increasing from 700 kilometers per hour to over 3,200 kilometers per hour.[1] Current turbine engines have been honed to a high level of efficiency, and therefore require significant effort for small improvements. Theoretically, achieving greater efficiency mainly involves running the engine with a higher compression ratio, higher combustion temperature, and at a lower weight. However, achieving these improvements is a more complex task, relying on many highly specified areas of study.

Gas turbine engines operate with three main systems: the compressor, the combustion section, and the turbine. Air enters the engine via the compressor, where it is pressurized and subsequently mixed with fuel in the combustion chamber. Combustion increases the temperature of the gas, at which point it expands in the turbine where its energy is captured and translated

into the rotational energy that continues to drive the compressor.

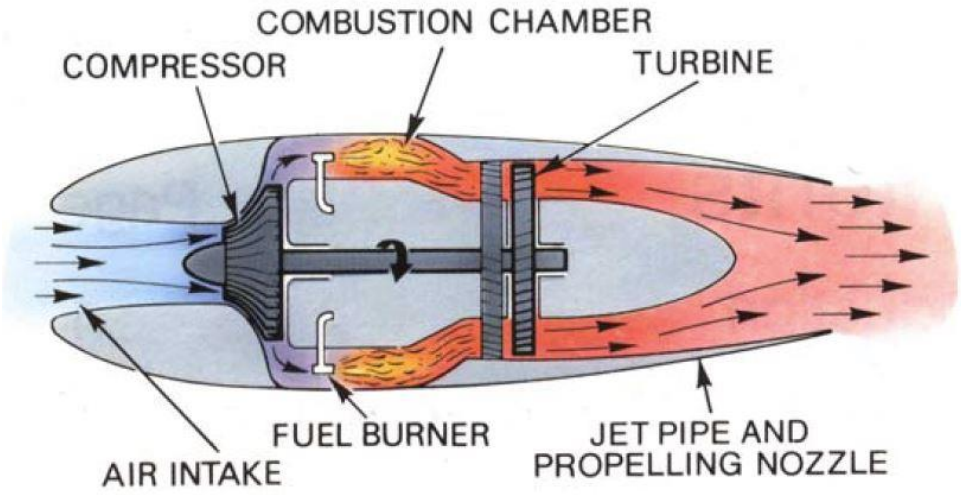

Figure 1-1: Basics of a gas turbine jet engine [8]

To understand factors that contribute to the efficiency of a gas turbine engine, it is first helpful to mention the Brayton cycle, which operates in essentially the same steps as the process described above. The governing equations of the Brayton cycle demonstrate that high compression and temperature ratios for air as it enters the combustion chamber maximize the efficiency of the cycle, and in turn, the engine itself.[2] Increasing the pressure and temperature in these sections, while improving efficiency, also causes higher stress on the engine components. Higher forces lead to faster fatigue of turbine blades, which is added onto by the degradation caused by higher combustion temperatures. Current temperatures in the hot sections of jet engines demand complex cooling mechanisms, ranging from cooling holes in the surfaces of individual turbine blades, coolant flow inside the blades, and thermal barrier coatings on the surfaces to help preserve the integrity of the base alloys. Further efficiency improvement can stem from weight reduction of engine components, especially in the case of jet engines, in which

less weight anywhere on the aircraft means less work for its engines. Creating more compact combustion chambers in particular can increase the thrust-to-weight ratio of an engine.[3]

The first turbine vanes to face the exhaust from the combustion chamber will be of primary concern to this research. Commonly referred to as first vanes, their interaction with highly turbulent flow fields is the main area of modeling and experimental observation. The architecture of this area of the engine, referred to as the 'hot section,' includes the combustion chamber and these first vanes.

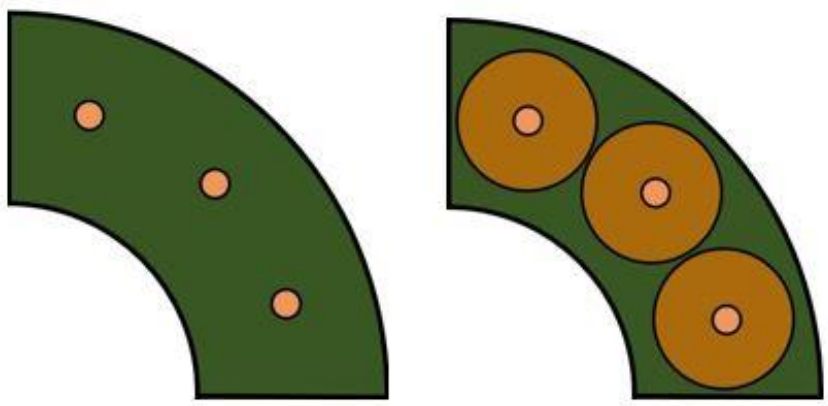

Figure 1-2: Annular (left) and cannular (right) combustor, both with light orange fuel injection nozzles and green annuluses, and cannular with dark orange combustion zones

There are various configurations of the combustor implemented in modern engines. Annular combustors, as are common in relevant jet engine applications, supply fuel to a relatively open combustion chamber through a series of nozzles spread along the annulus. Cannular combustors supply fuel into separated 'cans' that are spread along the annulus, in each of which combustion takes place. The annular setup, while lighter than a cannular alternative, leads to less predictable fuel distribution as well as the irregular flow structures that drive this research.[4] Figure 1-1 highlights very simply the conceptual differences between these setups. Ignition of the fuel-air mixture initially takes place with the help of an igniter, placed just downstream of one of the fuel injection nozzles. The spacing of these nozzles allows the flame to

spread throughout the annulus, at which point combustion continues during the entire cycle of operation of the engine.

Cooling of the combustion chamber takes place through various strategies, including thermal barrier coatings, effusion cooling, and impingement cooling, amongst others.[5] Effusion cooling is a method that carefully spaced holes in the liner wall to create a film cooling flow to protect the base metal in the liner. This method contributes to the overall cooling and near-wall behavior throughout the combustion chamber, but does not heavily influence the larger structures relevant to this work. While it is less aimed at cooling the combustion chamber, lower temperature dilution air also enters the stream of the exhaust and attempts to normalize the turbulent flow structures that later interact with the turbine blades.

The first vane itself employs carefully designed geometry for optimized cooling, aerodynamics, and heat transfer mechanisms in order to withstand the direct barrage of hot air from the combustion chamber. These vanes incorporate coolant flow inside the vane structure, film cooling through holes on the vane surface, as well as thermal barrier coatings on the on outer surface of the vane to combat their extreme operating temperatures. Acceleration and turning flow generate mechanical forces on these blades, which necessitates their structural integrity. The unsteady structures that interact with the vane can also create varied heat transfer on its surface.[6] For example, when pockets of fuel-rich air that did not combust initially move towards the vane, their late ignition can cause extreme heating on concentrated portions of the vane, which commonly referred to as hot streaking. Hot streaking is already the subject of a large body of literature, and is just one way in which uneven heating of the vane takes place. The interaction with irregular flow fields and development of coherent structures in the combustion chamber itself is the main focus of the work at hand.

Dilution jets supplying cooling air into the combustion chamber create wakes as they disturb the crossflow. Complex vortices form from the boundary layers in these wakes, sending irregular and unsteady structures downstream towards the first vane.[7] By understanding the structure of the flow and its effects on the vane, further work can be done to improve vane design and efficiency.

The work in this investigation was primarily computational simulation. The initial goal was to develop an understanding of both the heat transfer and flow field at the first vane with incoming turbulence in a standard setup, based on prior research. Consulting the computational and experimental setup and results of previous work, a base model was generated for computational simulation. From this point, the model was altered by changing the position of dilution holes in the combustion chamber in order to predict these effects on the first vane. Simulations were created for both stream-wise and circumferential shifts of the dilution holes. Finally, the effects of these changes were studied and analyzed to gain an improved understanding of varied dilution flow on vane flow fields and heat transfer.

Chapter 2 reviews the literature providing background information for this work, ranging from broad studies of turbulent flow field measurement, to studies of dilution jet mixing, to the most closely related background work on which the initial computational simulations were based. The model setups, including which models were studied, the development of grids in Pointwise, and the details of computational cases run in Ansys Fluent, are the focus of Chapter 3. The results of these models are laid out in Chapter 4 and are followed by an analysis of their meaning and overall conclusions in Chapter 5.

Chapter 2

Literature Review

This review is generally structured to follow air as it moves through the hot section of an engine, first looking at studies done in relation to the combustion chamber, then focusing in on dilution jet mixing, and next examining literature pertaining to first vane heat transfer and flow fields. Finally, the MS theses of both Sachin Vakil and Sarah Stitzel are closely reviewed as they served as direct predecessors to this work. The details of Vakil's experimentation and Stitzel's computational setup and are especially pertinent as they gave starting parameters for the base model presented in Chapter 3.

2.1 Combustor Flow Field Analysis

Different styles of combustor, such as cannular and annular, display varied flow fields within the combustion chamber and upon exit. While there is a broad literature available on modeling flow through combustors, this review will narrow its focus slightly. In order to focus on the most highly irregular flows created in combustion chambers, mainly modeling of annular combustors will be discussed here. It is also noteworthy that this work is based on non-reacting flows, which is not a constant among all combustor modeling. Combustion increases the temperature of the main airflow into the turbine section, however the structure of the flow can be accurately approximated in a non-reacting setup. As the turbulence in the flow is the main concern, and not the temperature gradient created by combustion, this is setup is appropriate.

Vakil and Thole highlight the differences between reacting and non-reacting cases, which principally deal with the accuracy of turbulence predictions.[4] With a three-component laser Doppler velocimeter and thermocouple rake, Vakil and Thole detected the presence of counter-rotating vortices that created kidney-shaped thermal fields in their large-scale experimentation. Though some disagreement is shown in the turbulence levels observed at the combustor exit between reacting and non-reacting cases, the larger factor in the accuracy of modeling flows was found to be the inclusion of dilution jets in the model. Consequently, dilution jets were a key component to Vakil's [8]and the present work, and will be discussed further in the following section.

Prior to Vakil and Thole's work, Barringer et al developed a large-scale flow simulator to focus purely on the exit of the combustion chamber.[9] His setup did not include a first vane cascade, as much later work would, and concentrated more on end wall conditions. Conclusions of the work supported further investigation of the flow exiting the combustor. While common practice at the time included assuming "either a constant total pressure field or a turbulent boundary layer approaching the turbine vane-endwall juncture," [9] the study proved otherwise with clearly defined pressure profile measurements. Another pertinent finding was the determination that turbulence length scales correspond to dilution hole diameter.

While non-reacting flow is more achievable to recreate experimentally and subsequently match to computational predictions, Mahesh et al were able to achieve suitable agreement between experimental data and large-eddy simulation (LES).[10] This approach was impressive in its capturing of complex geometry of the entire combustor system of a jet engine, though it focused on a much larger portion of a jet engine than the current research. More recent work

from Koupper et al used LES to study mixing and turbulence in the combustion chamber itself. However, this work focused on recreating accurate conditions to simulate hot streak generation rather than the physical behavior of the unsteady structures present.[11]

Computational models were also put to test in analyzing swirl in a gas turbine combustor in the work of Benim et al.[12] The work included both LES modeling and computational models based on shear stress transport (SST) more similar to the work at hand. While it was found that LES provided the most accurate computational results for predicting swirl in the combustion chamber, it was also concluded that coarser grids, more to the degree of the grids from the work at hand, could have practical use in predicting larger scale behavior in the combustor.

2.2 Dilution Jet Mixing Effects

A significant amount of research has been done determining the effects of dilution holes on combustion chamber flow fields. The earlier studies looked at a jet or rows of jets entering a confined crossflow. Further work has been done to understand the structures and temperature gradients resulting from jets in crossflow, as well as more specific studies on dilution holes and their resulting mean flow fields. All of this prior work is crucial to the current work in that it allows a better understanding of the types of structures that move from the combustion chamber and interact with the first vane.

In 1976, Holdeman and Walker presented a study of a row of cooling jets entering a crossflow observed the resulting temperature gradient and levels of jet penetration. They determined that jet penetration and profile uniformity was influenced both by jet diameter and

spacing, though the momentum flux ratio had the most influence on these areas.[13] Holdeman et al. moved this work forward with studies that considered flow and geometry more representative of a typical gas turbine combustion engine. Determining the combustor exit temperature gradients again was a main influence of this work while flow structures, which are more of the current focus, were less central. However, conclusions regarding spacing of jets and duct height in cases including opposing rows of jets provided valuable information for dilution hole geometry moving forward.[14]

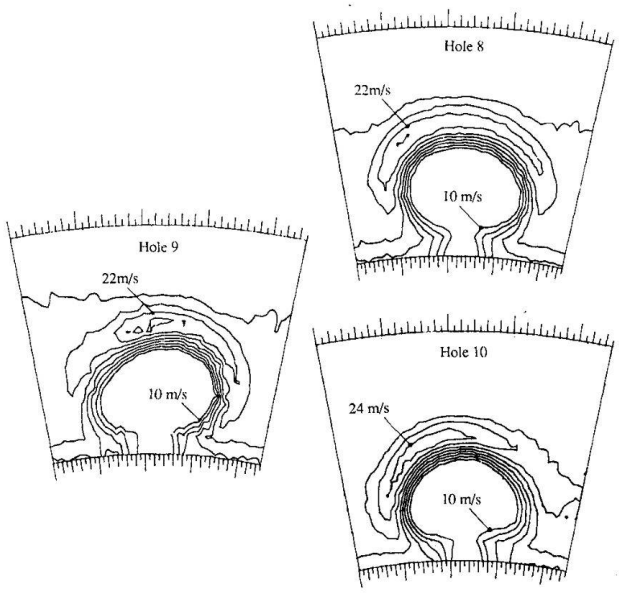

Figure 2-1: Axial velocity distribution irregularities [15]

Experimental work from Stevens and Carrotte observing the mean flow fields of dilution zones brought to light the complexity of the flow exiting dilution holes, both in flow structure and temperature uniformity. An example of the varied dilution exit plane velocities can be seen in Figure 2-1 below. The lack of symmetry among exit profiles of dilution jets gave important information that supplied further explanation of flow fields downstream of the jets. Among their conclusions about effects of these irregularities was the observation that the dominant double-

vortex structures resulting from the mixing jets contained vortices with varying strengths.[15]

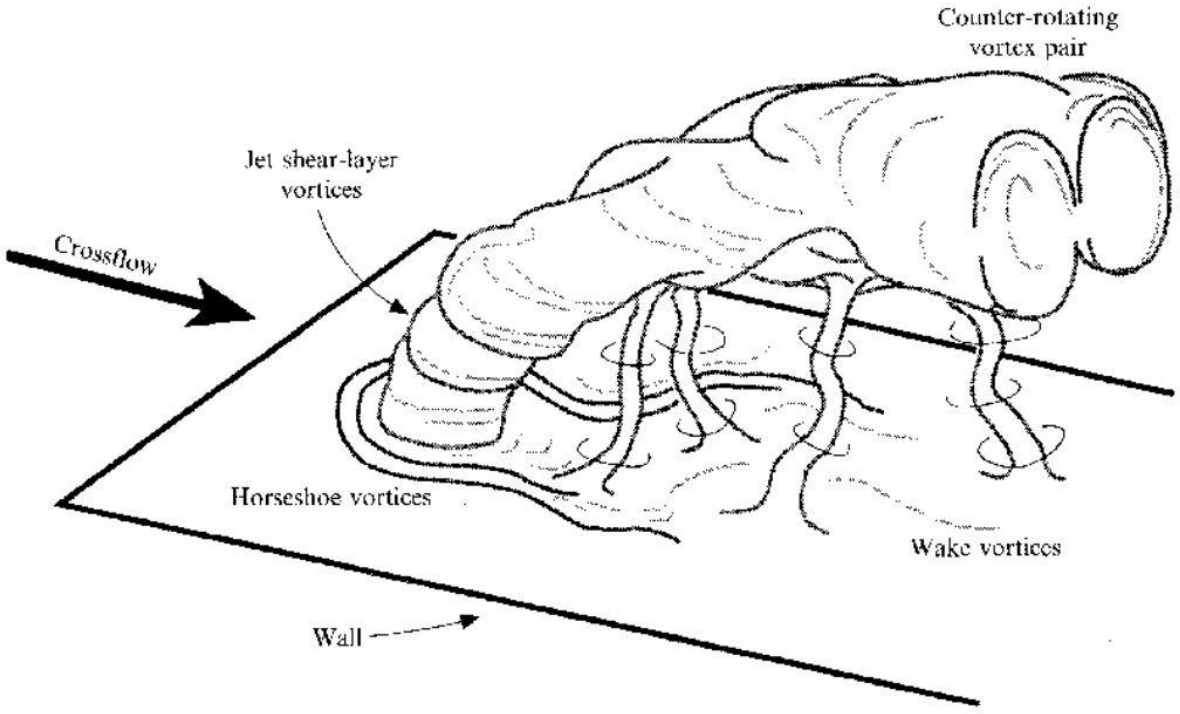

Figure 2-2: Vortical structures arising from a jet in crossflow [7]

The continuation of this study delves into dilution jet development, taking into account the irregularities presented by the earlier work. This continued work asserts that the annulus from which dilution flow enters the combustion chamber has a direct influence on the exit flowfield and trajectory of each jet entering the combustion flow,[16] though this finding is not fully reflected in the work at hand as it pertains more to temperature distribution at each hole. Furthermore, Stevens and Carrotte reaffirm the necessity of studying dilution flow effects using multiple jets entering a confined crossflow, as there are substantial differences between such a setup and earlier setups simply observing a single jet in unconfined crossflow.

Focusing more on the physics and structure of these phenomena, Fric and Roshko discuss the basic vortical structures resulting in introducing the flow of a transverse jet, including jet shear-layer vortices, horseshoe vortices, counter-rotating vortex pairs, and wake vortices. Figure

2-2 above provides a rather classic visualization of structures resulting from a transverse jet in crossflow. The major assertion of this work surrounds differentiating wake vortices that arise from a fluid jet in crossflow from those arising from similarly shaped solid bodies. Unlike flow around a solid body, which separates from the object to create vorticity, "wake vortices have their origins in the laminar boundary layer of the wall from which the jet issues".[7] This work enhanced the visual understanding of these structures immensely, as well as suggested improved experimental methods for their measurement. Smith and Mungal followed in this study, enhancing the experimental measurement techniques and refining some of Fric and Roshko's results.[17]

Returning more to gas turbine combustor representative work, Liscinsky et al completed an experimental study focusing on the mixing of jets into confined crossflow.[18] This work confirmed the setup for optimum mixing, as described by:

$$C = \left(\frac{S}{H}\right) * \sqrt{J} \qquad \text{(Eq. 1)}$$

where *C* is mixing effectiveness, *S* is spacing between orifice mid-points, *H* is the height of the duct at the injection plane, and *J* is the momentum flux ratio between the jet and mainstream. Continuation of this work observed both experimentally and computationally factors affecting jet penetration, which is critical to the overall mixing. One of the more relevant conclusions surrounded the variation of vortices created by in-line dilution configuration versus those created by staggered configurations, all in regards to mixing of the flow downstream.[19] Uncertainties of the downstream effects drive the varying of dilution hole placement in the work at hand.

In a study more focused on computationally representing dilution systems, Priere et al. [20] examine the agreement of LES and experimental work with jets in crossflow, moving more specifically towards the work at hand than the earlier discussed study by Mahesh. Images

produced, such as in Figure 2-3 below, demonstrate the higher level of focused detail in these computations with noticeable resemblance to experimental and conceptual images. The study also carefully considers mesh resolution and turbulence injected into flow, two extremely relevant factors for the work at hand. While this work with LES has a far greater resolution in the region of the dilution jets entering the main crossflow, the current work focuses its resolution on the first vane, which will be discussed in the coming section. The major conclusion of Priere et al. was the confirmation that this type of computational simulation could provide significant benefits for future combustor design in industry.

Figure 2-3: Example of jet visualization from large-eddy simulation [20]

2.3 First Vane Heat Transfer and Flow Field Studies

The literature surrounding heat transfer on turbine first vanes and flow fields around the first vane is generally large, however many studies separate the topics more than in the intent of this work. There are numerous studies of various cooling schemes or end wall conditions and subsequent heat transfer on the first vane due to these schemes. Similarly, a number of studies exist which model flow around the first vane. However, less work has been done to combine these two areas and find the heat transfer effects of the unique flow field exiting the combustion chamber and near the first vane. This is a central purpose of the work at hand. This section will

examine prior work leading to the current study, both in regards to vane heat transfer and the relevant flow field.

Ames examined the heat transfer effects of large scale high intensity turbulence on a turbine vane. Various inlet turbulence levels were measured in a four vane cascade and revealed the role of the length scale in determining the heat transfer at the stagnation region, where the heat transfer coefficient is highest, and surface heat transfer.[21] Length scale was also carefully calculated for inlets in the current work, though all computations were run at low turbulence (1-2%).

More recently, Qureshi et al. completed a study more representative of the current work which investigated vane heat transfer with swirling flow from a combustor. Computational predictions were made and experimental work was done using a cascade of vanes and a swirl generation system. The results characterize the boundary layer along the vane surface gathering in specific areas and dissipating in others, leading to uneven loading of the vane surface.[22] The Nusselt number along the vane surface is accordingly also varied in such cases with swirl, though end wall heat transfer remains fairly consistent between uniform and high swirl inlet conditions.

Moving more towards the structure of flow at the first vane, Rockwell describes vortex-body interactions, looking closely at the loading produced by the collisions of these flows with bodies such as turbine vanes.[6] The work provides confirmation that current computational models can provide sound insight to vortical structures and loading. Furthermore, it posits that control of vortex-body interactions is possible through low amplitude oscillation, however such

Figure 2-4: Schematic of stator vane test section [23]

control falls outside of the interest of the work at hand.

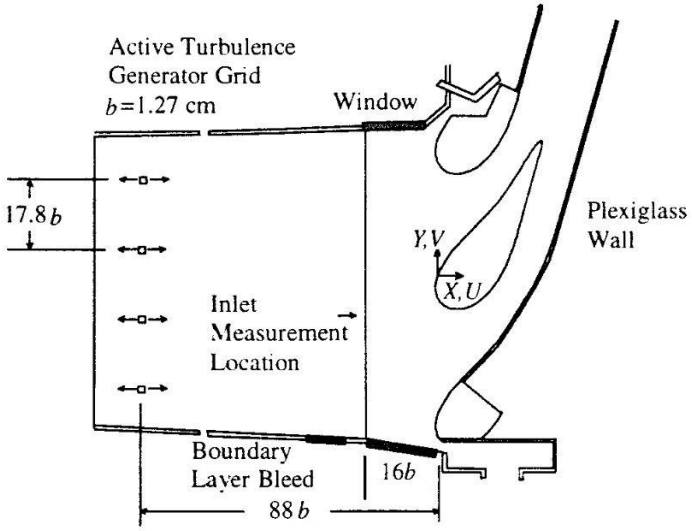

Figure 2-5: Schematic of stator vane test section [23]

Radomsky and Thole focus on rendering the turbulent flow as it passes through a cascade of first vanes, with the eventual goal of determining the heat transfer effects of this flow on vane surfaces. Experimental data showed consistently turbulent flow throughout the vane passage. Furthermore, high turbulence increased surface heat transfer on the high pressure side of the vane.[23] Such findings paved the way for a closer study of flow structures at turbine first vanes, and the experimental setup, seen in Figure 2-4, even resembles the direct predecessors of the work at hand.

2.4 Summary of Prior Work

Over the last 40 years, significant improvements have been made in the understanding of turbine jet engines, bringing many more of their intricacies to light. Previous experimental work simulating behavior in combustion chambers has made it clear that flow exiting this portion of

the engine is far from uniform and steady. Computational studies have been validated and further confirmed these conclusions, helping to predict complex areas of flow to guide new experimentation. It is also clear that dilution jets have appreciable effects on flow in the combustion chamber, which are also carried forward towards the turbine first vane.

The first vane itself has been the focus of a large body of work, both in regards to flow structures it induces and the heat transfer on the vane surface. However, little work has been done to meld these areas by examining large-scale structures created by dilution jets entering the combustion chamber and analyzing their effects on first vane heat transfer. This is the goal of the current research.

Chapter 3

Modeling Development and Setup

This main work involved in this research was the computational modeling of a wind tunnel used for prior experimental work. The wind tunnel from the research of Vakil [8] represents the combustion chamber and portion of the first vane cascade. The basic configuration of the current work recreated the geometry and conditions from Vakil, and then altered the location of the dilution holes in the basic configuration to determine the thermodynamic effects in mixing and on the first vane. In total, three distinct configurations were modeled and run through computational fluid dynamics (CFD) programs with two sets of parameters to observe the desired effects. The overall modeling process can be broken into the following steps:

-Create a SolidWorks model of the wind tunnel section for modeling

-Import the model into Pointwise to create a distinct mesh

-Load the mesh into Fluent to set the operational parameters and run calculations

-Complete post-processing of data in Tecplot

As the SolidWorks models for the wind tunnel had been developed prior to the start of this work, the steps to recreate them will not be discussed at length here. Only minor changes to these models were made to create new configurations. Also, post-processing of data will be discussed more closely in Chapter 4. The focus of this chapter will be discussing the background of the basic model, the mesh generation for the models in Pointwise, and running the subsequent calculations through Ansys Fluent. This should provide ample information for the recreation of this work.

3.1 Initial Model Background and Setup

The initial computational model developed in the work at hand is intended to closely model the conditions shown in the experimental and computational work of Vakil [8] and Stitzel [1] respectively. Side by side, these studies provided a set of data regarding flow fields and thermal characteristics throughout a combustor simulator, as well as matching computational predictions in the same simulator. The implications of these studies, in particular of Vakil's work, have been mentioned in section 2.1 above. However, this section summarizes the extent to which the current setup was developed based on details from these experiments and computations.

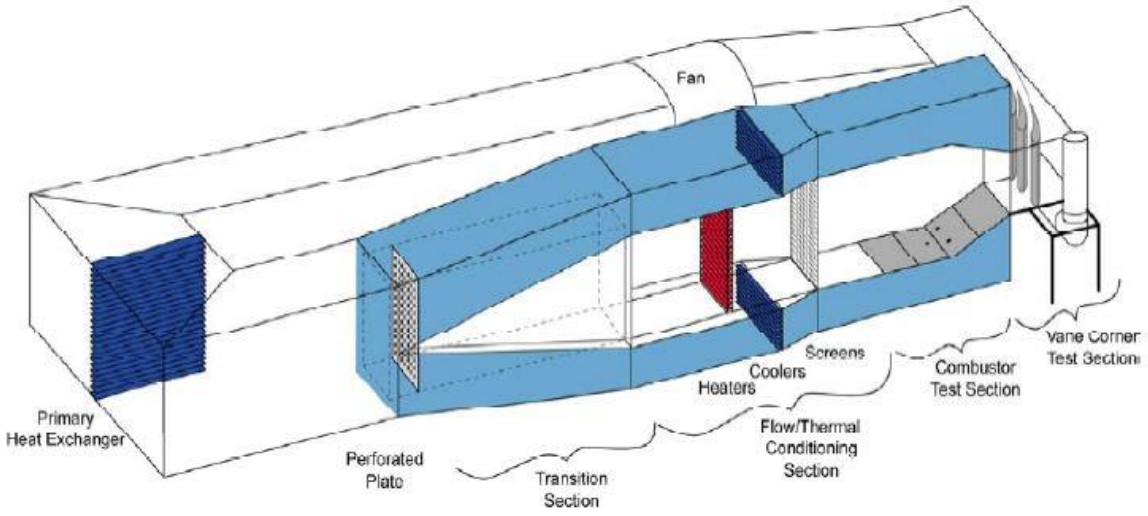

Figure 3-1: Large-scale, low speed, closed-loop wind tunnel schematic from Vakil [8]

The experimental setup which the current work models is structurally and geometrically very similar to the wind tunnel setup of Vakil, shown in Figure 3-1. The model created from this schematic basically begins with an inlet surface located where the screens are placed towards the

end of the Flow/Thermal Conditioning section. The dimensions match exactly those from Figures 3-2 and 3-3, which show the tunnel from above and the front side, respectively.

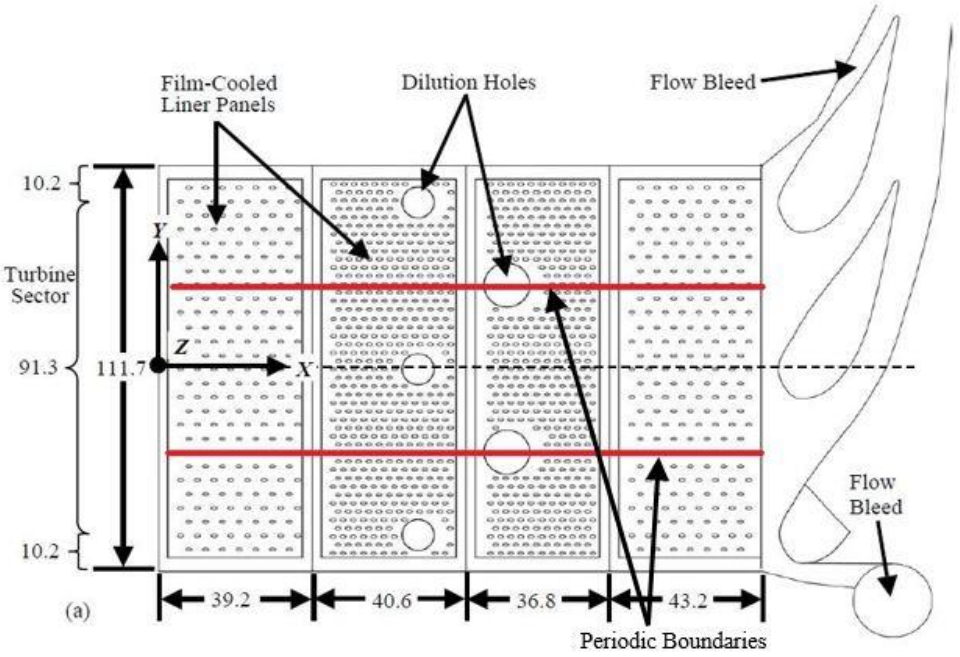

Figure 3-2: Vakil schematic top view, red lines indicating periodic boundaries [8]

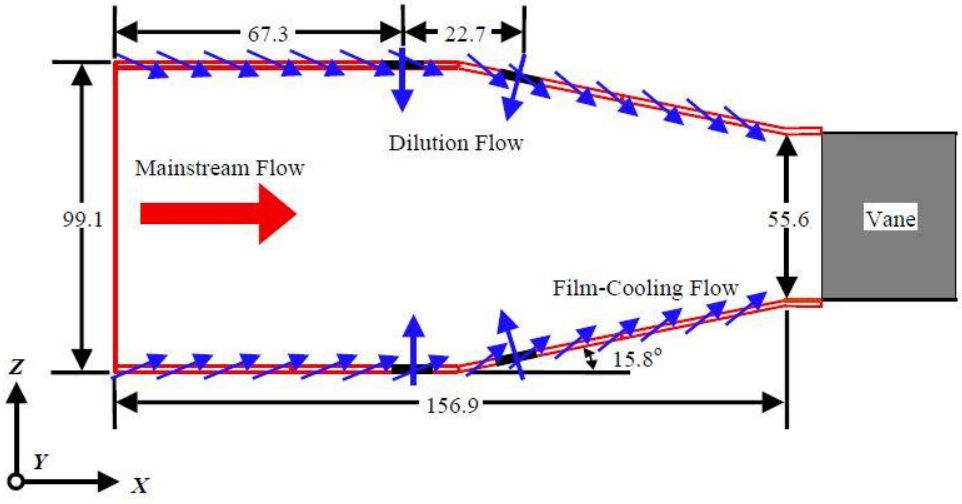

Figure 3-3: Vakil schematic side view with X, Y, and Z axes for reference [8]

The red lines in Figure 3-2 mark where the section is sliced in the current simulation, in the stream-wise direction through the centers of the second row of dilution holes, to create periodic

faces in along the x-z plane. While not shown by the red lines, these periodic faces extend into the vane cascade and split the area between vanes so that only a single vane is modeled.

Table 3-1: Number of holes, and diameter from Vakil study [8]

	Number of Holes	Diameter (cm)
Dilution Row 1	3	8.51
Dilution Row 2	2	12.12

Dilution hole sizes were defined using the values from Table 3-1, which was created with values from a corresponding table in the full thesis of Vakil. To see this, and other full tables from Vakil and Stitzel, see Appendix A. The work at hand did not simulate the panels for film cooling, the detail for which the tables in Appendix A include in detail. Though film cooling certainly influences wall temperatures, the focus of this study was on the vane surface and large structures created by dilution holes, on which the film cooling holes have little appreciable effect.

The product of these specifications can be seen in Figure 3-4a. below. The two variations below it change the position of the dilution holes. Figure 3-4b. includes a shift of both rows of dilution holes 50 percent closer to the first vane, while Figure 3-4c. includes a span-wise shift of the dilution holes by half of a combustor pitch. These changes were intended to investigate the specific effects of the location of dilution jets in relation to first vane heat transfer. Moving the jets closer to the vane or positioning the second row dilution hole in line with the leading edge of the vane were two changes that could not only provide potential benefits to combustor design (i.e. through decreased combustor size or lower heat transfer rates) but could also help gauge the overall effects of dilution jet structures on the first vane.

The rectangular prisms attached at each dilution hole entrance represent coolant supply plenums. These take the place of the entire coolant flow sections shown in light blue in figure 3-

1 above, and allow for a controllable amount of mass flow to enter each dilution hole. The plenum dimensions are consistent with each other wherever possible, though there are exceptions to ensure that their walls do not overlap with either the main tunnel geometry or other plenums. These differences are inconsequential, as the plenums were sized to have an inlet face more than 5 times the dilution hole area, so that the supply flow was truly a plenum (very low speed) condition.

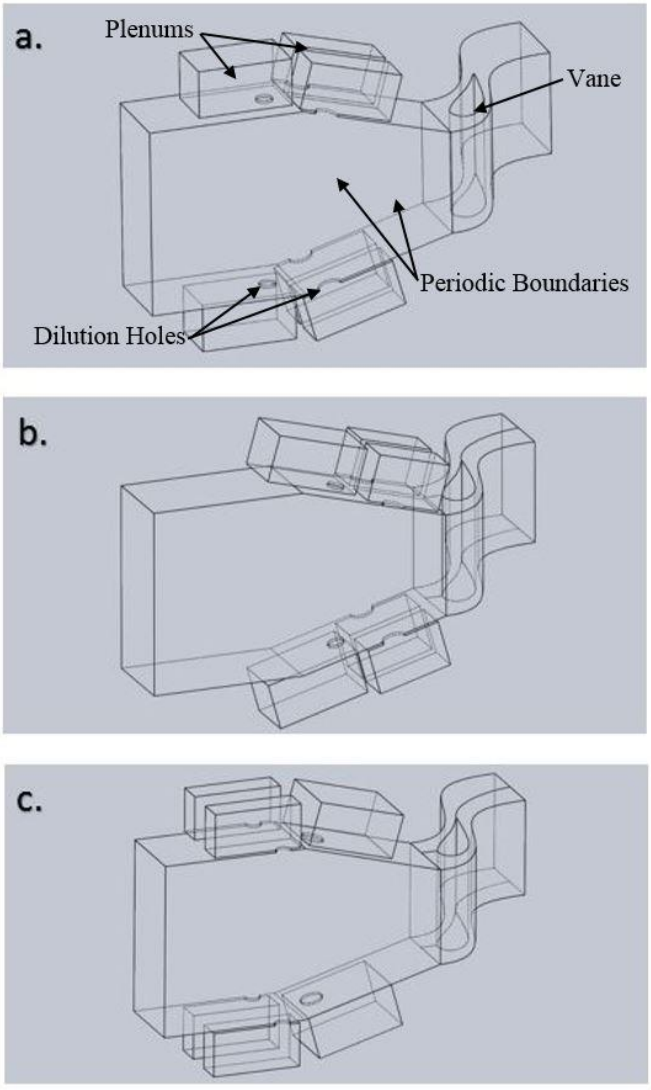

Figure 3-4: SolidWorks models of periodic wind tunnel section a) basic configuration from Vakil b) dilution holes shifted to 1/2 distance to first vane c) dilution holes shifted 1/2 pitch span-wise

After these models were completed in SolidWorks, they were converted to Parasolid files (.x_t file extension) to be imported into Pointwise, the grid generation software.

3.2 Mesh Generation

Although many CFD software packages, including Ansys Fluent, have their own capabilities for meshing parts prior to running their analysis, Pointwise is far more precise and robust. With grid generation as its sole purpose, it allows for a much greater degree of control when determining grid type and areas of greater focus throughout the model. The purpose of this step in the overall process of CFD is to aid with the development of finite volumes. Generating a grid over all of the surfaces of the model helps to break it into numerous far smaller pieces that are analyzed individually when calculations are run through Fluent.

As a standalone program, Pointwise has some unique terminology and a general methodology for grid generation. To start, while the terms ‘grid’ and ‘mesh’ have been used interchangeably to this point in this thesis, Pointwise more exclusively uses ‘grid.’ The imported part, which appears in Pointwise as a wireframe model (see Figure 3-5) is called the ‘database.’ Standard convention for grid generation in Pointwise is as follows:

-Map connectors to all of the lines of the database

-Fill connectors with points

-Create 2-dimensional surfaces, called ‘domains,’ from areas enclosed by connectors

-Create 3-dimensional shapes, called ‘blocks,’ from volumes enclosed by domains

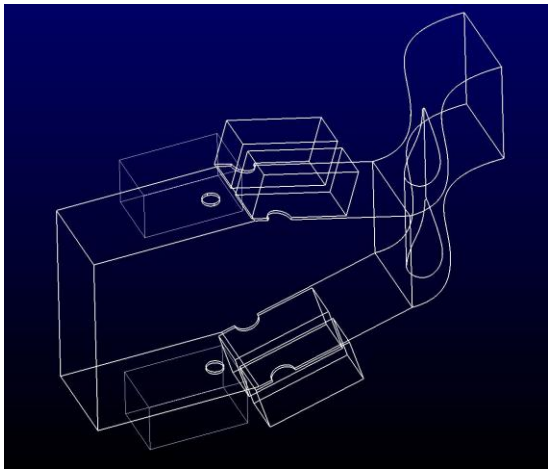

Figure 3-5: Basic configuration database

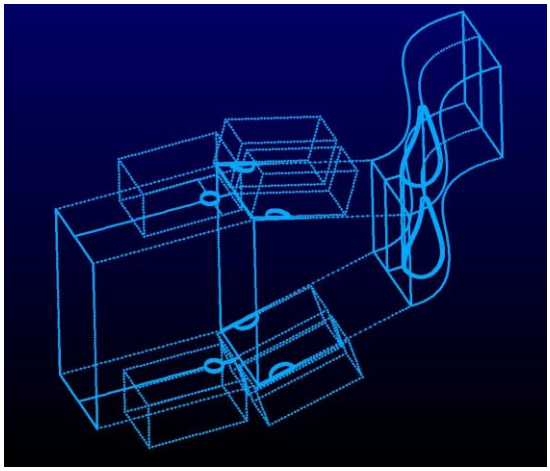

Figure 3-6: Connectors with points

When a database is imported from SolidWorks, it creates the wireframe based on the separate features used when constructing the model. It also incorporates features such as split lines, as can be seen in Figure 3-4b. and 3-4c. above with a curve leading from the trailing edge of the first vane to the midpoint of the top edge of the tunnel exit. When these features, or others, are not present in the database, they can be added as connectors using the Create/Draw Curves tool in Pointwise. However, depending on the complexity of the feature to be added, it may be easier to incorporate it into the original SolidWorks model. It is for this reason that the curved split lines were included in later variations of the SolidWorks model for this work.

After importing the database, the “Connectors on Database Entities” tool turns each segment from the wireframe into an empty connector. At this point, any entities missing from the database that will be needed to create domains later should be created. For example, the dilution holes split by the periodic boundary can be observed to be missing connectors that would close the semicircle. In Figure 3-6, there are connectors present at those locations that were added in Pointwise.

Filling connectors with points is the first way to influence the quality of the grid in specific areas. In this research, the vane is of primary concern, and therefore the connectors that make up its outline have the highest density of points. Furthermore, the spacing of points along a connector can be altered manually, which made it possible to concentrate a high number of points at the stagnation point on the leading edge of the first vane, as well as at the trailing edge.

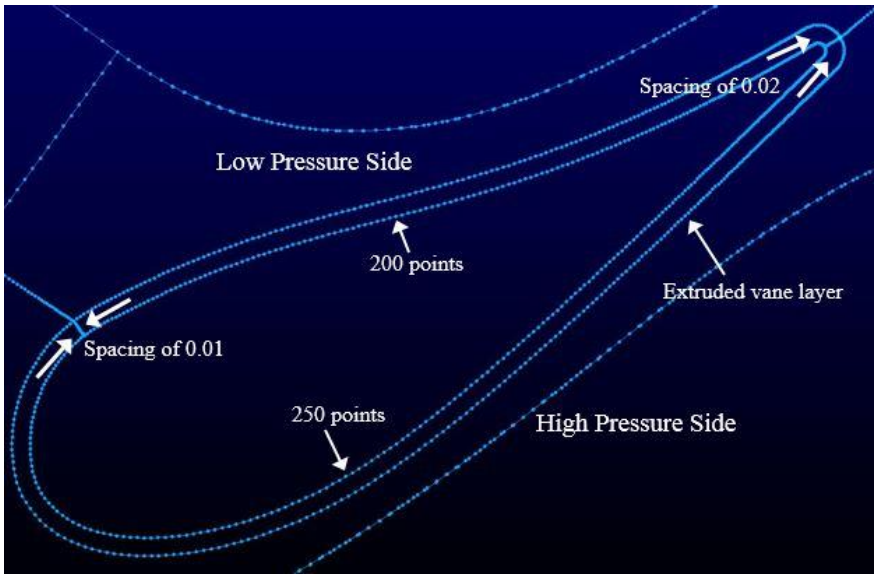

Figure 3-7: Details for populating first vane connectors

In order to ensure consistency from case to case, the number of points and their spacing on connectors was documented. The details of the connectors creating the vane geometry can be

seen in Figure 3-7. Pointwise also tracks the number of points and spacing along each connector in the “List” panel, which can also be used to select and edit these details.

The second ring around the vane profile comes from the extrusion of the domains that cover the vane surface. Extrusions will be discussed later, however domain construction is the next step in the overall grid generation process.

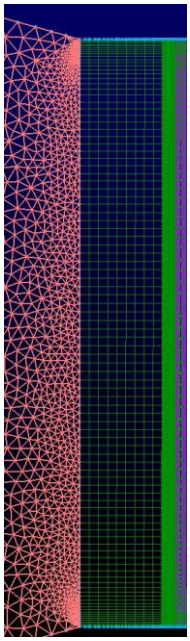

Figure 3-8: Transition from highlighted unstructured grid to structured grid at vane inlet

Creating domains is a matter of selecting the connectors that enclose an area and using the Assemble Domains tool buttons. Domains can be created in two styles: structured and unstructured. Structured domains provide traditional rectangular grid faces, while unstructured grids populate faces with a more random assortment of triangles. A grid with solely structured domains is referred to as a ‘structured grid,’ and likewise a grid with solely unstructured domains is an ‘unstructured grid.’ When both are used, as was done for all of the configurations of this work, the grid is called a ‘hybrid grid.’ The contrast of structured and unstructured domains can be seen in Figure 3-8, while the entire set of domains is shown below in Figure 3-9.

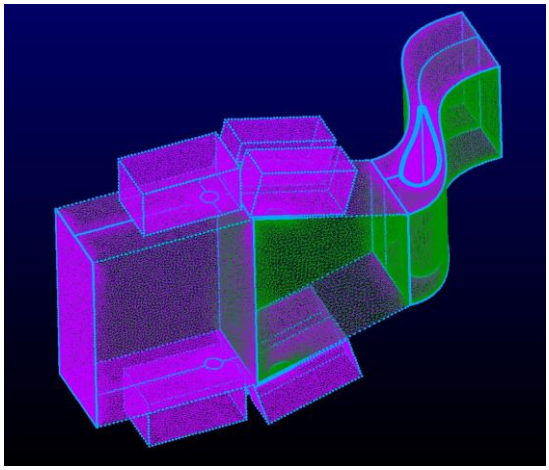

Figure 3-9: Domains covering all model surfaces

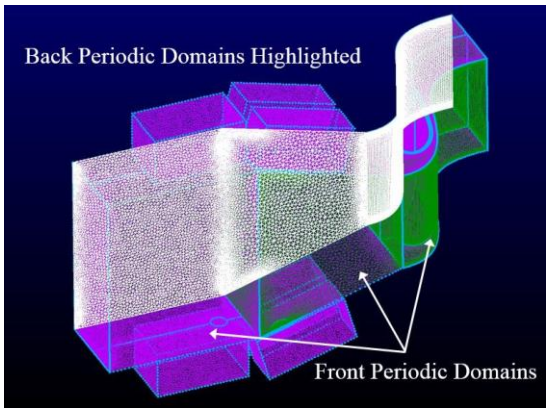

Figure 3-10: Front and back periodic domains

The rationale for using a structured grid is that it typically allows for much higher resolution and accurate calculation, however it can be difficult to adapt to complex geometries. In that sense, unstructured grids are slightly more robust as they more easily account for rounded or asymmetrical connectors. However, they can also lead to poorer aspect ratios and generally lower overall grid quality. In the cases at hand, a hybrid grid was chosen to obtain high levels of detail around the vane but also to lower grid size in areas of less interest, such as the plenums. In the vane section of the model, the front, back, vane inlet, vane surface, and outlet faces all contain structured domains while the top and bottom walls contain unstructured domains. This

was intended in part to help create a slightly higher resolution throughout this portion of the model with the structured domains, as well as to accommodate the curving and varied geometry with unstructured domains along the top and bottom wall.

As the model represents a periodic section of the wind tunnel, the domains on the front and back 'periodic' faces were developed as such. This entailed making sure any connectors that make up part of the front periodic face had equal numbers of points and spacing with their counterparts on the back face. Once the front domains were made, Create/Periodic was used to create the translational periodic faces.

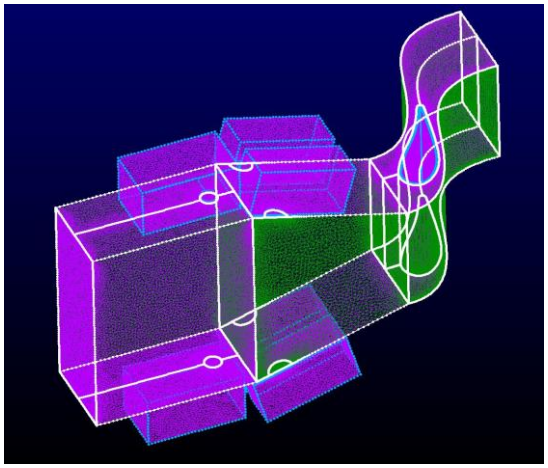

Figure 3-11: Central 3 blocks highlighted

After domains have been created, blocks can be formed. Blocks are made by selecting the domains which enclose some volume, and then are solved by Pointwise to fill these volumes with either rectangular prisms or tetrahedrons for structured and unstructured grids, respectively. If a block has both structured and unstructured faces, the block will be solved as an unstructured block with tetrahedrons. The cells filling these blocks are not graphically displayed, though the outlines of the blocks making up the main section of the wind tunnel are shown in Figure 3-11.

As mentioned previously, structured blocks are desirable for areas with high resolution. In order to obtain a structured block around the vane surface, the surface was covered

with a structured domain. Then, prior to constructing other domains, the domains on the vane surface were selected and then Create/Extrude/Normal was used to build 30 repeated layers of the domains, created a structured block with extremely fine resolution close to the vane surface. The height of the first cell on the surface of the vane, or any wall, is measured by the y-plus value. This refers to the non-dimensional height of the first grid point, and for a good quality resolution should be less than 1. Table 3-2 specifies the conditions used for creating the exact extrude from this work.

Table 3-2: Specifications to recreate extrusion

Extrusion Details	
Initial Delta-s (inches)	0.0004
Growth Rate	1.2
Extrusion Method	Algebraic
Boundary Conditions	Constant Z
Steps	30

Once the all domains have been created and solved, the grid is considered complete. The size of the grid varies dramatically in number of cells based on the style and high resolution areas. The basic configuration shown in these figures contains about 8.3 million cells, while earlier, more complex iterations contained closer to 15 million cells.

The first step in preparing the grid for CFD is to examine various aspects of its quality to ensure it will run without error in Fluent. The Examine option has a variety of capabilities for checking grid quality. Low average skewness values in categories such as “Skewness Equiangle” help to ensure the grid will function properly in Fluent. If a large enough portion of cells contained skewness of over 0.9, convergence of the solution in Fluent became unlikely. Figure 3-12 shows a cut displaying skewness equiangle. The area near the low pressure side of the vane and the top and bottom walls presented the most challenges with skewness, as cell size changes

relatively rapidly in a small space. Changing grid style, the number of points on a connector, or their spacing are all possible ways to alleviate high skewness or poor aspect ratios.

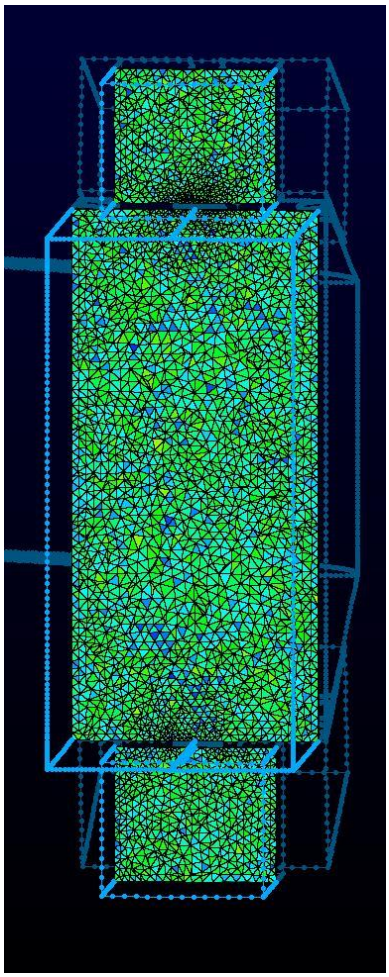

Figure 3-12: Equiangle skewness cut on the Y-Z plane near combustor main inlet

Once the grid is of suitable quality, the CFD solver can be selected from a list of programs including Ansys Fluent. After selecting the solver, boundary conditions can be specified for whichever domains require them. As the labeling of the boundary conditions carries over from Pointwise to Fluent, a naming convention of some sort is required to ensure the boundary conditions can be set to the correct parameters prior to running CFD calculations.

The system for naming boundaries on each of these models started by moving through the major features of the model in the direction of air flow. Also, for simplicity, a maximum of

two words (or acronyms) were used in each name. For example, the first features named were "main inlet," "top wall," "bottom wall," and "vane." It is also worth noting that multiple domains can be included in a boundary, as was the case for most boundaries.

Numerous plenums and dilution holes called for a set of acronyms to help define the location of each. The 3 sets of location references created to differentiate these features were

1. forward/rear
2. top/bottom
3. front/back.

The first letter of each of these words was used when necessary, and always with the sets appearing in the same order (1, 2, 3). For example, the plenum inlet boundary on the forward, top, back plenum was listed as "ftbplen inlet." A full list of these conditions can be seen in Table 2 in Appendix A.

The boundary types in the models reflected the relatively simple flow conditions with most boundaries set as "Walls." The plenum inlets were treated as mass flow inlets as these conditions were specified in Vakil's work, while the main inlet was set to a velocity flow for the same reason. The periodic faces were set as "Symmetry" faces, however this would be modified in Fluent to create periodic surfaces on the main wind tunnel sections. The periodic faces of the plenums were allowed to remain symmetrical, as this was a better representation of the flow through a complete dilution hole.

With all of the necessary boundary conditions defined, the model could be exported to Fluent as a case file, where the remainder of the computational setup took place.

3.3 CFD Setup and Parameters

The final setup and computation for the models is completed in Ansys Fluent. Pointwise converts grids to case (.cas) files that Fluent uses to set up the parameters for a calculation. Due to the grids being developed in inches in Pointwise, the initial step upon opening each case was to use the Scale menu to convert to metric.

The General panel of the menu was critical for determining mesh quality with both the Check and Report Quality options. Issues such as negative volume cells and poor orthogonal quality could halt entire cases with divergent solutions. In each of these menus, it was necessary to apply any changes suggested by warning messages to complete successful calculations.

The overall method modeling turbulence throughout the cases was the Reynolds-averaged Navier-Stokes (RANS) approach, based on solving for Reynolds stresses in a steady case. This varies from other methods such as LES, discussed in Chapter 2. Models specified in the Fluent setup included the Energy model and SST k-omega viscous model. The SST k-omega turbulence model has been used previously in the ExCCL lab for vane and blade computational studies. The specified y-plus value on the vane surface of approximately 1 was required to use this turbulence model to obtain accurate flow information near these walls.

The Materials menu allowed further definition of air properties and the models for calculating its properties throughout the simulation. The density of air was defined by using the incompressible ideal gas assumption, while air viscosity was calculated by the Sutherland model.

Defining boundary conditions allowed for two variations of each case to be run for each of the three models. These variations were focused on determining different heat transfer effects throughout the air flow and on the first vane. In the first variation, all wall boundaries, including the vane walls, were defined as adiabatic surfaces and the freestream temperature differed from

the coolant flow temperature. This revealed the temperature gradient throughout the wind tunnel due to mixing of the flows. The second variation assumed a single air temperature in both the freestream and coolant flows and defined a heat flux of 2000 W/m^2 on the vane wall in order to determine the heat transfer coefficient on the wall surface.

The flow conditions in the simulation followed the typical operation of the tunnel in Vakil's work, as seen Tables 3 and 4 in Appendix A though some of those parameters were not needed for the computational model. Mass flow through the dilution holes was calculated based on the percent of mass flow addition listed in Vakil's work, and remained constant throughout the cases. Table 3-3 lists the operating conditions used in both variations of each case in this work. Note that dilution hole mass flow is defined for full dilution holes, meaning that the holes split by the periodic walls used half of the listed value at their mass flow inlet.

Table 3-3: Parameters for both simulation variations

	Adiabatic Vane	Non-Adiabatic Vane
Freestream Temperature, T∞ (˚C)	59.04	59.04
Coolant Temperature, Tc (˚C)	22.55	59.04
Main Inlet Velocity, U∞ (m/s)	1.6	1.6
Forward Dilution Mass Flow per Full Dil. Hole (kg/s)	0.1356	0.1356
Rear Dilution Mass Flow per Full Dil. Hole (kg/s)	0.10855	0.10855
General Wall Heat Flux (W/m^2)	0	0
Vane Heat Flux (W/m^2)	0	2000
Forward Dilution Flow Momentum Flux Ratio, Jf	198.3	177.1
Rear Dilution Flow Momentum Flux Ratio, Jr	12.1	10.8

At the mass flow and velocity inlets, turbulence was specified by intensity and length scale in all cases. Based on low turbulence values from Stitzel and Vakil, the main inlet turbulence intensity was set to 2% and the turbulent length scale was calculated by multiplying the diameter of the vane leading edge by 3, giving a value of 0.35304 meters. The turbulence at the plenum mass inlets was set to 1 percent, and the turbulent length scale was calculated in the

same way, referencing dilution hole diameters. This resulted in turbulent length scales of 0.2553 meters and 0.3636 meters for the forward and rear sets of holes respectively.

To first run through each case, the SIMPLE scheme was used for pressure-velocity coupling, while first order solutions were used for all spatial discretization. Once a first order solution had been established, each case was run through again with second order calculations to reach a converged solution. In order to aid in reaching the first order solution, the under-relaxation factors for pressure and momentum listed in Solution Controls were lowered to 0.2 and 0.5 respectively.

To help gauge the progress and convergence of each solutions, a similar set of monitors was developed for each case. These mostly included area-averaged pressure and velocity readings for various surfaces throughout the model, such as the main outlet, the vane inlet, the vane surface, and a mid-span plane. Figure 3-13 below shows a plot of the average pressure on the vane surface approaching a final value of near -187 Pa over 2000 iterations.

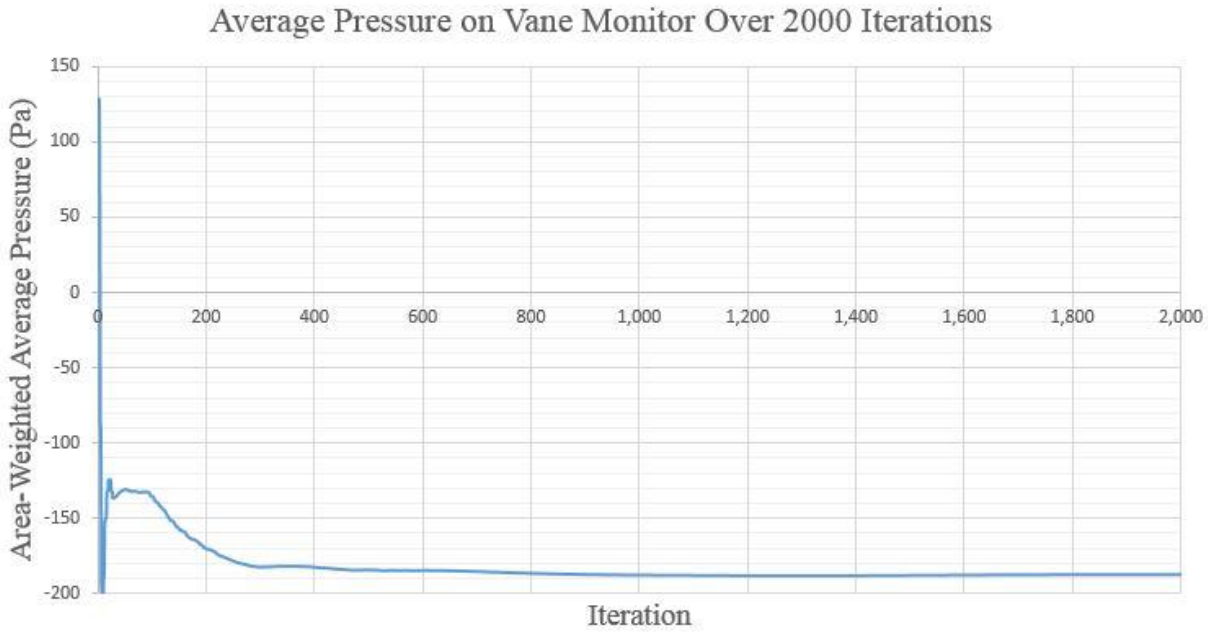

Figure 3-13: Monitor data convergence for vane pressure over 2000 iterations

The final step before running each calculation was initializing the solution. While there are two basic methods for initializing, hybrid and standard, the models that successfully ran through hybrid initialization succeeded in running without divergence in every case, making it a good indicator of the grid quality. The process automatically runs through ten iterations and attempts to find a basic initial convergence of the solution.

Once this process is complete, the case was set to run for typically 2000 iterations for a first order solution, followed by another 2000-4000 iterations with second order solution methods. Viewing various contour and vector plots in the Results menu allowed for confirmation of a physically sensible solution. Further confirmation came from viewing the monitors as discussed above and checking the levels of residuals for the main aspects of the solution. Once monitors had converged to steady levels and the residuals became low enough, the cases were considered complete. A screenshot of completed residual values is seen below in Figure 3-14, showing acceptable continuity near the order of 10^{-3} and values closer to the order of 10^{-5} for velocity. Typical residuals for the energy equation were lower, on the order of 10^{-8}, as shown here.

iter	continuity	x-velocity	y-velocity	z-velocity	energy	k	omega
3991	5.5883e-03	2.8337e-05	2.7565e-05	3.4344e-05	1.0565e-08	1.0493e-04	7.7236e-06
3992	5.5858e-03	2.8347e-05	2.7556e-05	3.4366e-05	1.0599e-08	1.0502e-04	7.7367e-06
3993	5.5872e-03	2.8359e-05	2.7549e-05	3.4386e-05	1.0565e-08	1.0513e-04	7.7498e-06

Figure 3-14: Example residual values for a case run a total of 4000 iterations

Chapter 4

Computational Model Results

After reaching an appropriate level of convergence for each case, the resulting data was loaded into the post-processing program Tecplot to create clear images of various aspects of each solution. The results of both variations for each of the three model configurations are discussed and compared in this chapter.

4.1 Basic Configuration Results

The flow through the basic configuration was intended to mirror that of the experimental flow in Vakil and in the computational results of Stitzel. While a detailed comparison of those studies is not done with the work at hand, the parameters shared between the three are intended to create a relatively standard setup as might be observed in industry. Two variations of this model were run: one with separate coolant and freestream flow temperatures and adiabatic wall conditions, and another with uniform flow temperatures and a constant heat flux on the vane wall. As the main purpose of the second variation was to determine the heat transfer coefficient at the vane wall, the first variation (with separate flow temperatures) will be the main focus of flow structure discussions across the three configurations. The second variation of each configuration will be considered in relation to the heat transfer coefficient and in case of any discrepancies. The main features of the solved computational model for the first variation of the basic configuration are discussed below, followed by comparisons to differences with the other configurations.

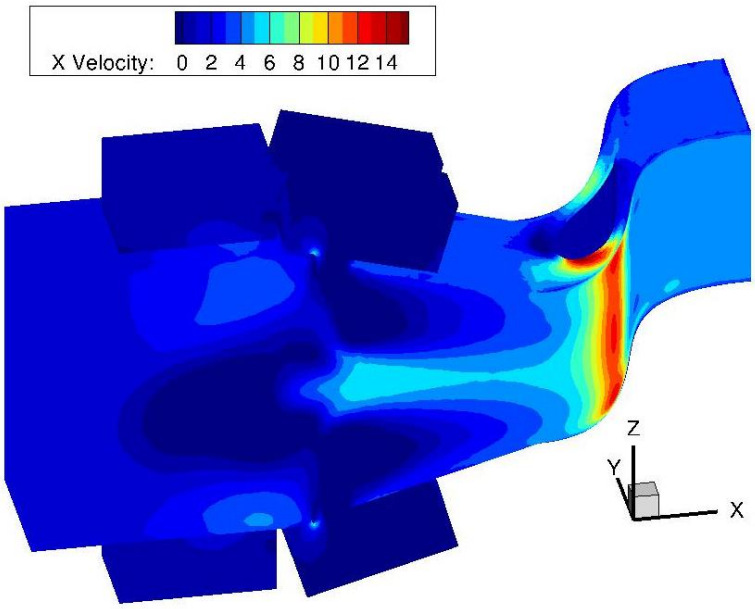

Figure 4-1: Contours of x-velocity in m/s at boundaries of basic configuration

Figure 4-1 is a contour plot displaying the x-velocity of flow along the boundaries of the entire wind tunnel geometry. This plot helps to visualize the stream-wise velocity throughout the tunnel. Air entering the tunnel from the main inlet has a uniform velocity of 1.6 m/s. As the first dilution jets enter the main flow, they initially add slightly to the x velocity. An area of stagnation can be seen where the momentum of the second row of jets, pointed slightly against the freestream, slows the x-velocity. The effect of the second row of dilution holes is also more pronounced in this plot as these jets are split by the periodic face that is shown, while the first row of dilution holes are in the center of the section.

After this stagnation area, and as the tunnel begins to constrict, the flow increases in velocity. When it reaches the vane, another stagnation point can be seen on the top wall at the leading edge, followed by higher velocity flows around both sides of the vane. As expected, the high pressure side of the vane shows lower velocities, while the highest velocities in the tunnel

are observed as the air moves around the low pressure surface of the vane. Finally, the flow evens out in velocity after passing through the vane cascade.

While the plot is labeled as showing the velocities at the boundaries of the model, this is not completely accurate. In reality, it shows the flow inside the first cells along these boundaries, as the flow at the surface of the wall boundaries has no velocity. Furthermore, the high y-plus values along the main walls also explain why the flow is not slowed as it would be if these first cells on the walls were small enough to capture the slowed boundary layer flow that exists very near these wall surfaces.

To further understand the physical structure of the flow, the x, y and z-velocity contours at midspan, the x-y plane that cuts through the tunnel at the middle of the vane, are shown in Figure 4-2 below. In this plane, the x-velocity behaves similarly as it does along the periodic boundaries and top planes shown in Figure 4-1. Some recirculation can be seen in line with the first row of dilution holes, followed by a speeding up of the flow near the second row and as the tunnel constricts. In this view, a slightly higher velocity can be observed moving towards the low pressure side of the vane, where the highest velocities are seen.

The y-velocity plot shows a generally lower level of flow in the y direction in the combustor portion of the tunnel. Air can be seen moving out of the center of the tunnel after the first row of dilution holes, but this movement is then tempered by the second row of dilution holes, whose jets push the air from the periodic surfaces back towards the center of the combustor section. Finally, as the flow passes the vane and the tunnel turns, the air gains a high level of y-velocity, as expected.

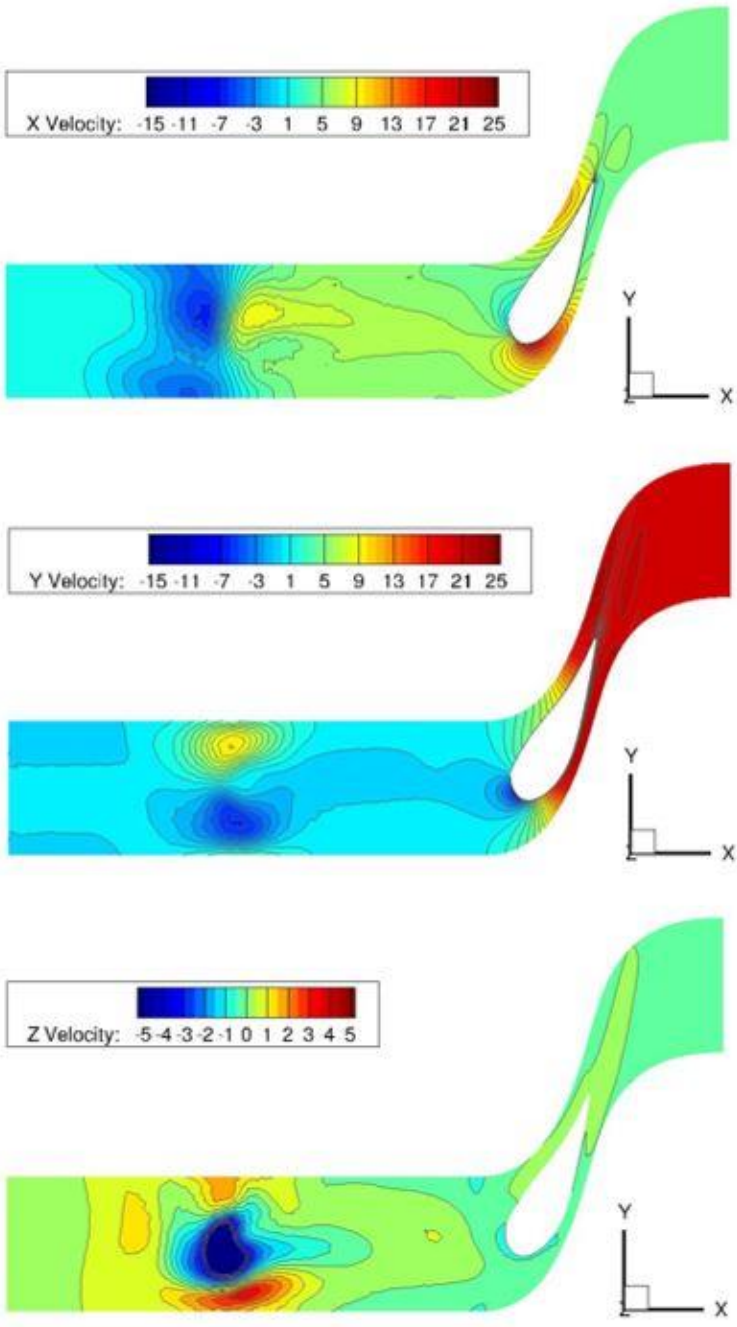

Figure 4-2: Contours of x, y, and z-velocity in m/s at midspan of the basic configuration

Velocity in the z-direction is notably less than in the x and y-directions, as shown by the smaller range of velocities. Furthermore, the z velocities at the midspan plane can be expected to be their smallest, as this plan is the maximum distance from all of the dilution jets, which shoot

in the z-direction. Most likely as a result of the recirculation zone that can be seen in Figure 4-1, there is some air flow in the negative z-direction, into the page, in the center region of the tunnel. Some air circulates upwards around this zone as well, before losing almost all z-velocity and moving towards the vane. After the vane cascade section, the flow experiences minimal z-velocity.

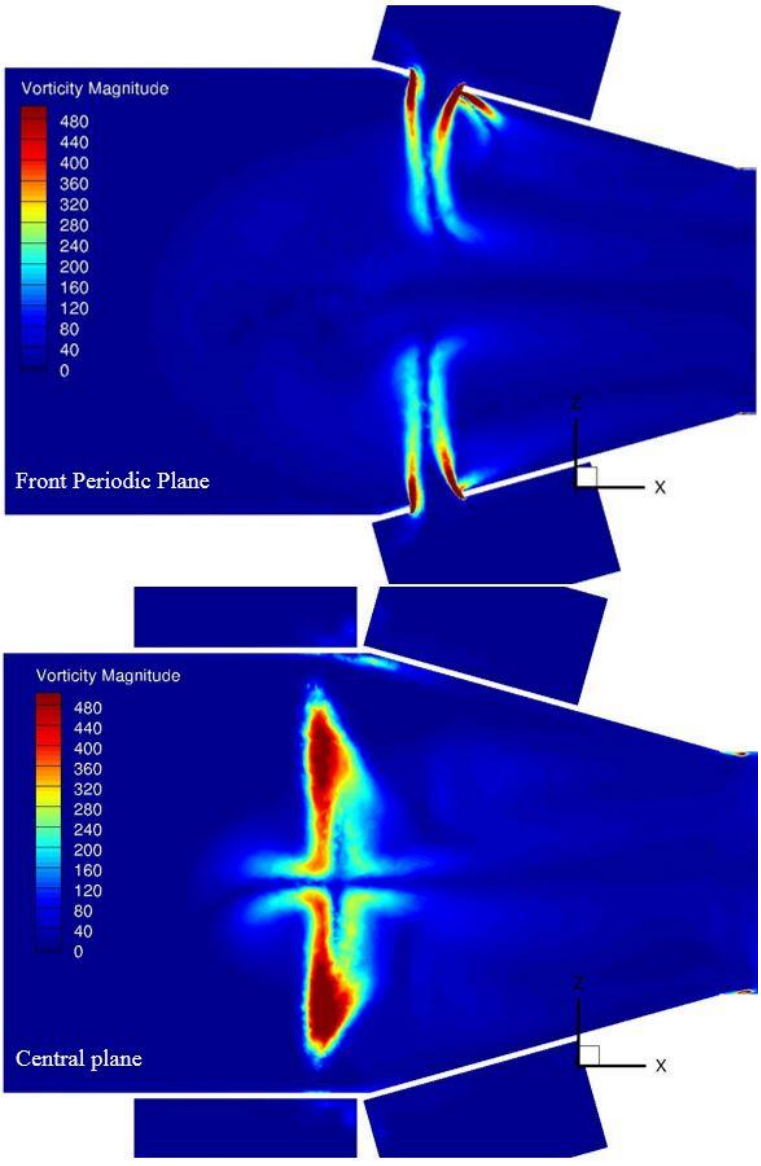

Figure 4-3: Contours of vorticity magnitude on front periodic and center planes

Aside from velocity, vorticity is another flow characteristic that gives insight into some of the behavior of the air as it moves downstream. Figure 4-3 above shows vorticity on x-z planes that cut through the two sets of dilution holes. The top image is along the front periodic face and shows the influence of the second row of dilution holes. Shear layers are formed between the high speed jets entering the slower crossflow, which creates high vorticities at the edges of the dilution holes. Light areas of vorticity also form downstream of these jets, which could include some of the structures discussed in Fric and Roshko [7]. The lower image shows the vorticity created by the first row of dilution jets. These jets appear to bend with the direction of the freestream flow quickly after entering. Large areas of vorticity develop directly in line with this row of dilution holes and most likely contribute to the recirculation area shown in this region by the velocity contours. On both planes, the vorticity created from the dilution jets does not persist far downstream as the flow approaches the turbine inlet.

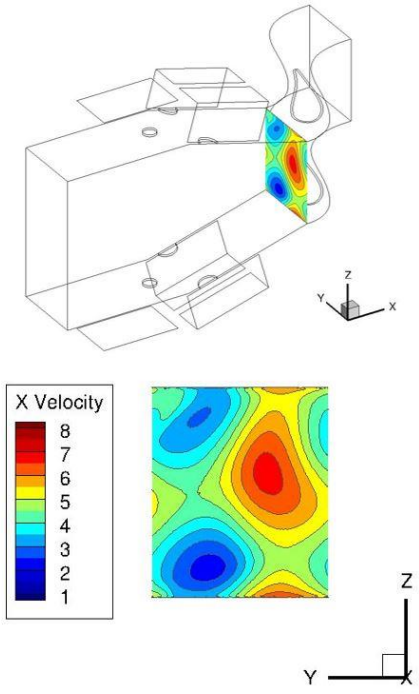

Figure 4-4: Contour of x-velocity in m/s at vane inlet plane with isometric view of entire tunnel

After developing a basic understanding of the flow through the combustor model, the focus will shift more to the flow and behavior of the model around the vane. Flow entering the turbine inlet helps demonstrate where the air will strike the vane itself. As the predominant velocity is in the stream-wise, or x, direction, Figure 4-4 displays contours of this velocity at the turbine inlet plane, with the top image clarifying the plane orientation. The region of the highest velocity can be seen to the right of the center of the inlet, towards the low pressure side of the vane. Flow is concentrated in this center stream where the air from the opposing dilution jets has converged, with some higher velocities towards the top and bottom of the inlet as well. Lower velocity regions accompany the high pressure side of the vane, and are more towards the top and bottom walls. It is also worth noting that this figure helps to demonstrate the periodic nature of the model, as the contours from the left edge of the plot can be seen to be continued on the right edge of the plot.

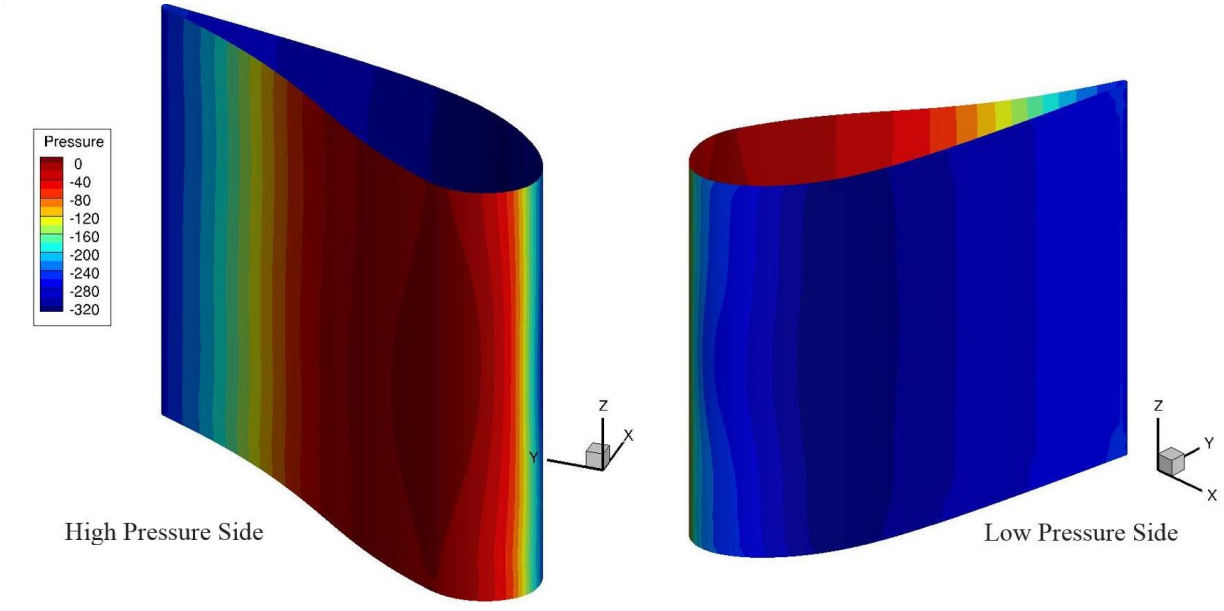

Figure 4-5: Contours of pressure in Pa on vane surface

Moving to the vane itself, Figure 4-5 displays the high and low pressure contours on the vane surface. This basic configuration displays a fairly uniform distribution of pressure,

especially along the low pressure side of the vane, where the contours create almost linear regions of pressure. The region of highest pressure is more rounded and larger around the center of the vane, suggesting a stagnation point located closer to midspan. After this region, pressure drops off in a more uniform manner as it approaches the tailing edge.

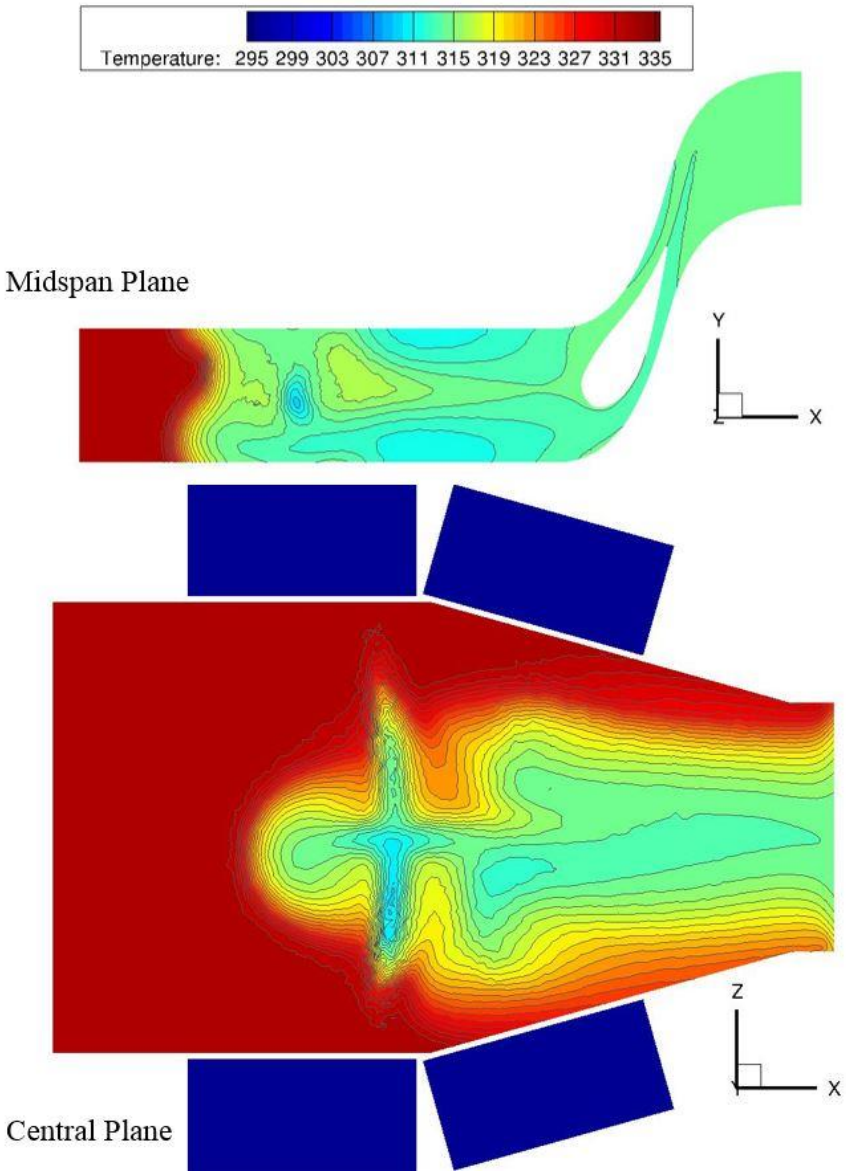

Figure 4-6: Contours of temperature in K from the midspan and central planes of the basic configuration

Temperature is the final aspect of the computation which will be examined here. In the basic configuration, the dilution jets are able to lower the temperature to near midway between

the freestream entrance temperature of 332.19 K and the coolant temperature of 295.7 K in the center third of the flow as it approaches the turbine inlet. Figure 4-6 depicts both a top view of the midspan plane and a front view of the center plane of the combustor section demonstrating the contours of temperature throughout.

The temperature profile of the vane in the basic configuration is seen here in Figure 4-7. As expected from the plots above, the center portion of the vane where the most mixing has occurred is closest to the average air temperature. Both sides of the vane have very similar temperature profiles, with the exception of the slightly higher temperature towards the bottom of the trailing edge on the low pressure side. This is possibly a function of flow generated from the endwall carrying hot fluid towards the trailing edge, similar to the effects seen along the top wall-vane interface.

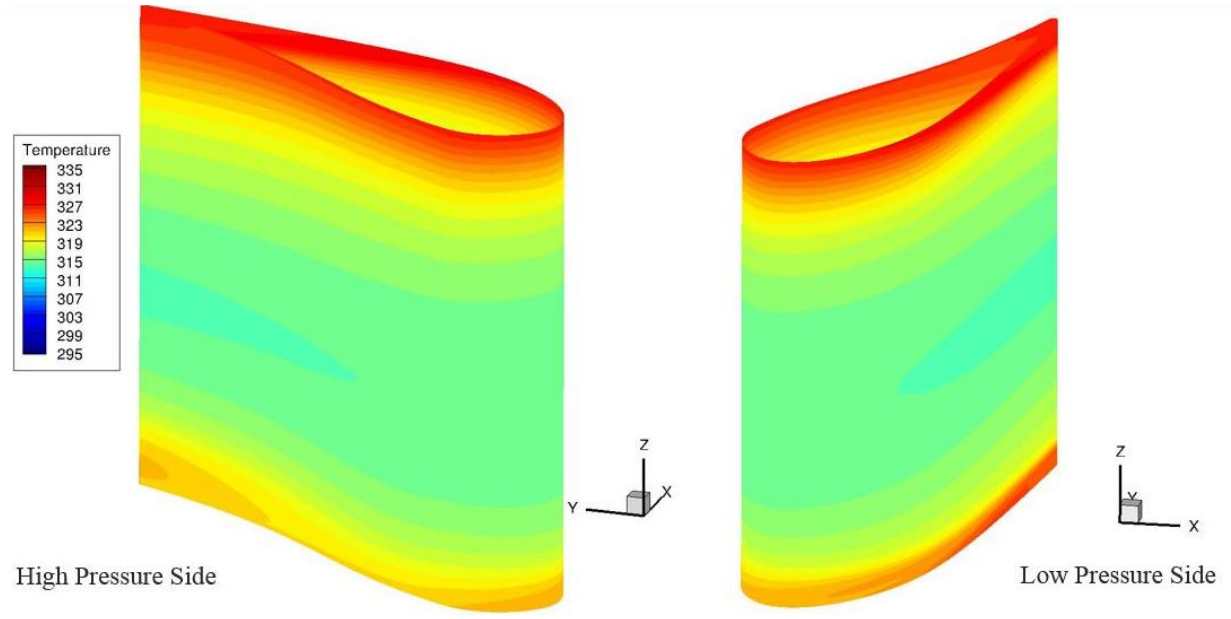

Figure 4-7: Contours of temperature in K on both sides of vane

4.2 Comparison of Varied Configurations

Shifting the placement of dilution holes to find their effects on vane heat transfer was the main intent of this research, which ran computational simulations of two variations of the basic configuration described above. In some aspects, the changes in placement had very little effect on the overall flow, however in others there were noticeable differences. For ease of description, the basic configuration will be referred to from this point as C1, the configuration with the dilution holes shifted 50 percent closer to the vane will be C2, and the configuration with the dilution holes shifted by a half of a combustor pitch in the span-wise direction will be C3. This section will comment on the similarities and differences in flow structure and give a side by side comparison of the heat transfer condition of the vane in each configuration.

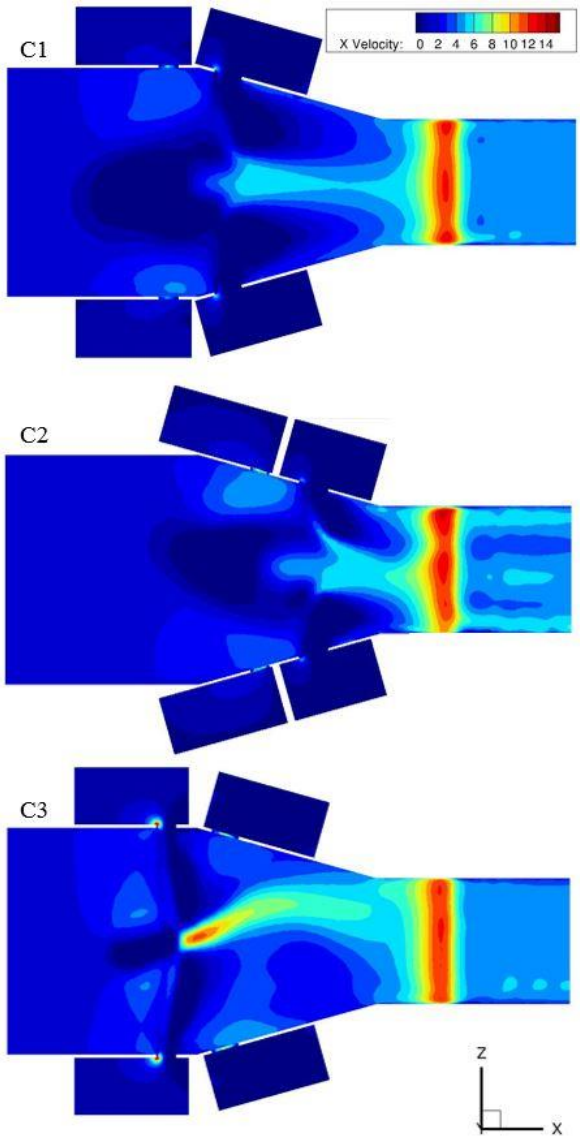

Figure 4-8: Contours of x-velocity in m/s for front view of C1-3

To gain a basic understanding of the major differences in flow, Figure 4-8 shows a comparison of x-velocities on front view of C1-3. Similar structures are visible in C1 and C2, only in a more compressed area in C2. The stagnation zones match fairly well between the two cases, and flow gathers and speeds up near the midspan region. As the jets in C2 are closer to the vane, it seems to push the higher x-velocities forward and even past the vane, whereas in C1 the vane serves to normalize the x-velocity for the most part.

C3 also demonstrates similar flow to C1, especially when considering the span-wise shift. Looking at the center plane of C1 would likely reveal a similar flow pattern to C3 in the combustor section, aside from the upward bend of the x-velocities. This is most likely a function of high residuals in the calculation, which may be evened out with more runs. The cases were run a total of 6000 iterations each, and it is unclear why C3 may have needed more runs to create a slightly more symmetrical solution, however it should not have had a major impact on the overall heat transfer effects. The bend in the flow aside, the main idea in this configuration was to observe the effects of the second dilution hole being centered on the vane leading edge, and not the flow in the combustor, which should remain constant with C1. Again as in C1, the flow in C3 is evened out after the vane, with relatively uniform x-velocities.

Plots of y and z-velocities similar to those shown in section 4.1 above were also created for C2 and C3, however they demonstrate similar comparisons in the main combustor portion of the tunnel as shown in the x-velocity comparisons. Likewise, equivalent vorticity plots were generated, however do not indicated differences aside from those mentioned above. They will not be discussed here, however these plots can be found in Appendix B.

The inlet velocity planes give more clear indications of the differences between the configurations as the flow in each approaches the vane. Figure 4-9 lays out the velocity contours from all three configurations with the x, y and z-velocities in each row and C1-3 in each column.

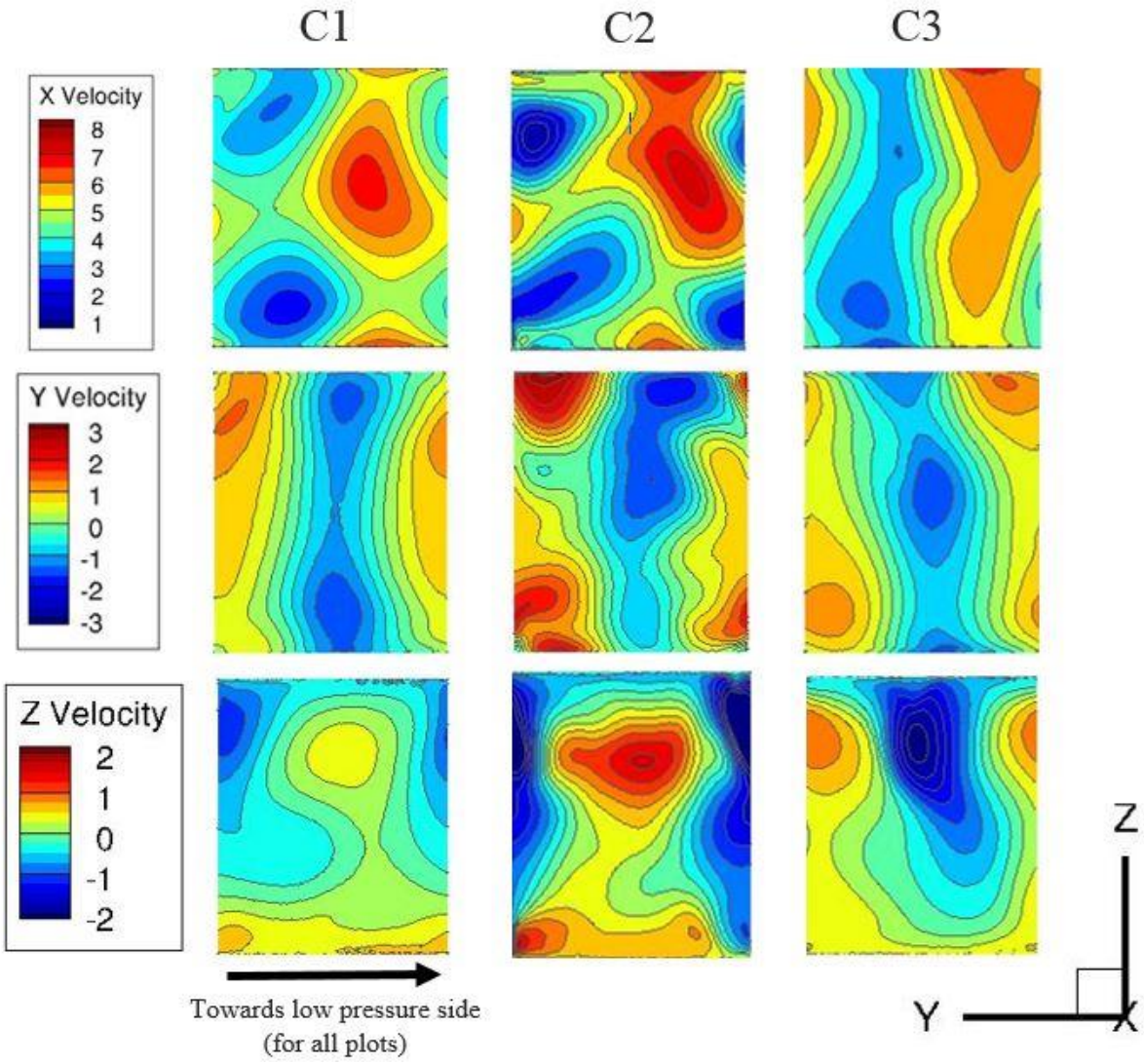

Figure 4-9: Contours of velocity in m/s at the turbine inlet plane across all configurations

General trends can be found across the contours for all configurations, however the magnitudes of the velocities tend to vary case by case. Across the x-velocity contours, higher velocities can be observed off-center towards the low pressure side of the vane. In comparison to C1, the velocities in at the inlet plane for C2 are more extreme and defined as the dilution holes

are were positioned much closer to the vane. C3 shows similar magnitude velocities to C1, however these are vertically distributed more evenly than in the other two configurations.

The y-velocity contours also display uniformity in the negative velocities flowing from the center of the plane towards the low pressure side of the vane. In C3, the effect of the upward bending stream in the combustor section is somewhat apparent, as the flow pattern from C1 appears to be similar only skewed slightly towards the top wall in C3. The plots of z-velocity show similar effects across the cases. Again, C2 demonstrates a greater magnitude than its counterparts, though it is noteworthy that the scale of the z-velocity is more focused than the y-velocity, which is in turn slightly more focused than the x-velocity scale. C1 shows a very low level of upwards z-velocity near the center of the plane, while C3 corrects for the upward bend with velocity moving downwards in the same area. Overall, these contours agree with the flow in the main portion of the combustor section.

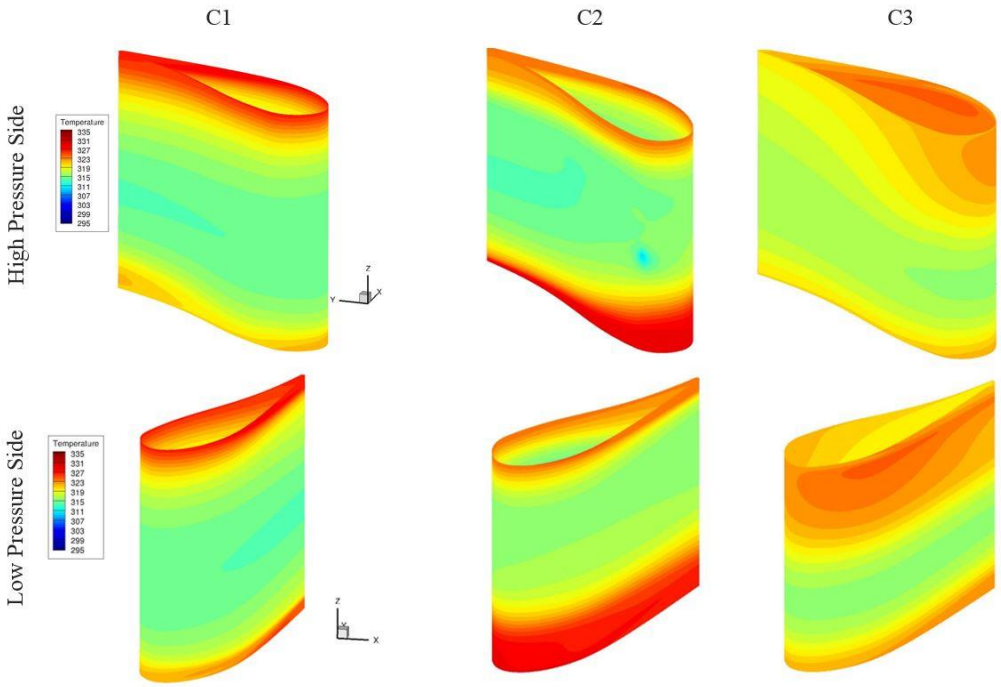

Figure 4-10: Contours of temperature in K on the vane walls for all configurations

Temperature contours throughout the combustor section demonstrate similar mixing effects to what each velocity profile would suggest. Regions clearly affected by the dilution jets in terms of vorticity and velocity also contain temperatures between T_∞ and T_c. See Figure B-4 in Appendix B for contours at the midspan of C2 and C3. These gradients help define the temperature contours at the vane walls in each configuration, which can be seen in Figure 4-10. The contours for C2 suggest a similar temperature distribution as seen in C1, however with higher temperatures near the bottom wall rather than the top. This is also a more lopsided distribution, with the high temperature region close to double the size in C2 compared to C1. Elsewhere, the temperature is fairly constant, with slightly cooler regions near the midspan height of the vane. C3 displays lower temperatures over the entire surface of the vane, with fewer regions containing concentrated higher temperatures. This may reflect the different structure of flow entering the inlet. There are higher temperature contours near the top and bottom of the vane, especially on the low pressure side, though these are more rounded than the banded high temperature regions in C1 and C2. Such differences suggest the differences also seen in the heat transfer coefficient on the vane surface.

The central comparison of these configurations arises in the determination of the heat transfer coefficient values. The heat transfer coefficient, h, describes the ratio of the heat flux of a surface divided by the change in temperature between that surface and the flow around it. It is measured in units of Watts per meter squared Kelvin. In this application, it helps to describe the areas of the vane which will experience greater levels of heat transfer, and thus undergo more wear over time. Figure 4-11 below shows the high and low pressure sides of the vanes from each configuration with contours of h values displayed on their surfaces.

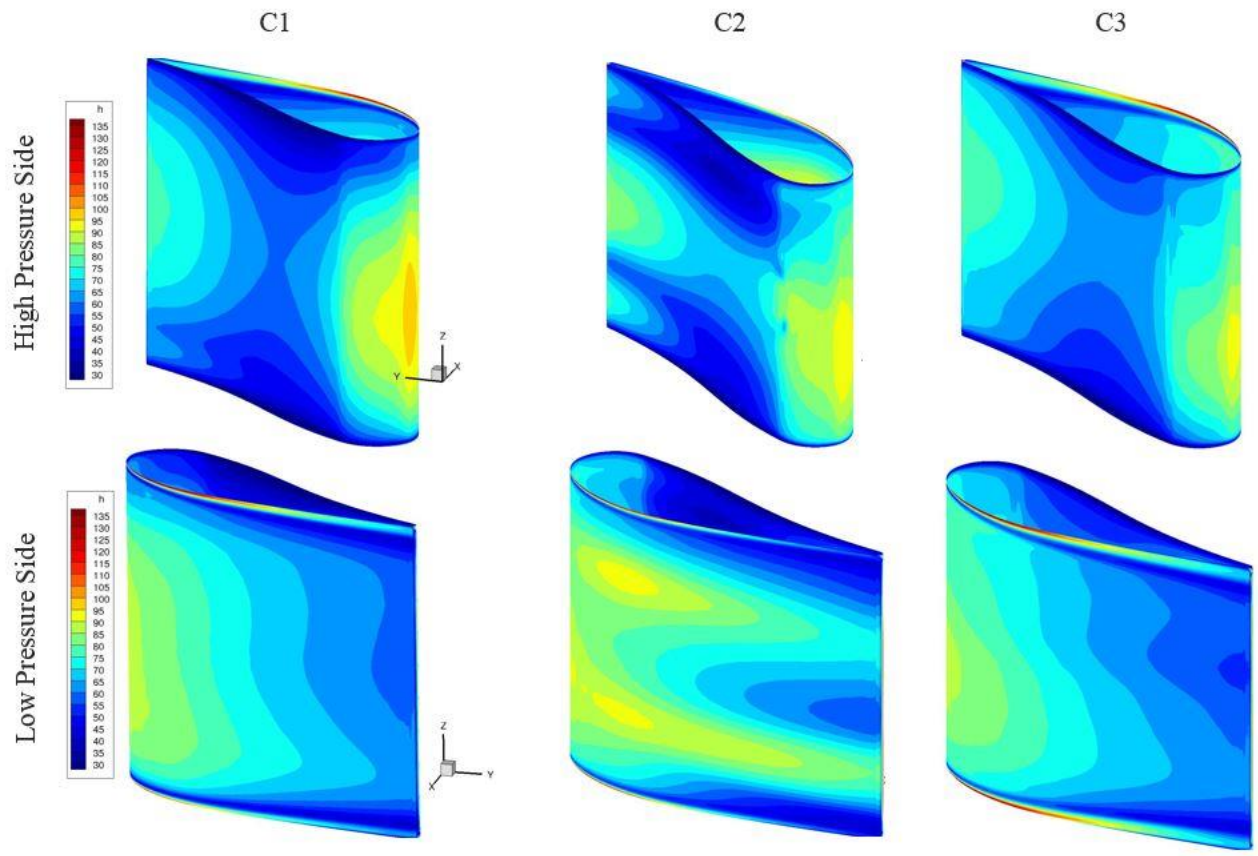

Figure 4-11: Contours of h values ranging from 30-135 W/m2K along vane surfaces for C1-3

The heat transfer from the standard vane setup is highest just below the midspan region on the leading edge, and stays highest at midspan along the high pressure side. On the low pressure side of the vane, the h values decrease more uniformly, with slightly higher values towards the lower half of the vane. Both C2 and C3 display better heat transfer performance at the leading edge, as the h values do not reach the magnitude of the highest values from C1. This is surprising for C2, as the higher velocities at the vane inlet might have suggested a more concentrated level of heat transfer along the leading edge. However, this is not the case, which may be the effect of the closer proximity of the cooling dilution jets.

While C2 does boast lower h values at the leading edge and comparable values on the rest of the surface, these values are far more sporadic. On the high pressure side of the vane, the contours follow a similar pattern to those of C1, however the regions of low h values are more pronounced, as is the region of higher h values near midspan. The low pressure side of the vane shows the same trend to an even more extreme level. Distinct regions of higher h values exist near the top and bottom of the vane, with lower values around the midspan level of the trailing edge. These harsh variations around the entire vane suggest unequal thermal loading and increase the probability of uneven thermal stresses on the vane from heating. While moving the dilution holes nearer to the first vane may save space in the combustor, it appears that it would also have damaging effects on the vane itself.

The changes in C3 however appear to have positive effects on the vane heat transfer. As mentioned previously, the leading edge has lower overall h values. These values also seem to be more constant along the leading edge. Both sides of the vane also display similar values to those of C1. The high pressure side of C3 shows decidedly less variation than C2, and appears to have generally smoother contours than C1. While C1 has one region in the center with lower h values than C3, it is possible that the smoother transition in C3 would be better for the overall vane performance. On the low pressure side, the pattern from C1 with lower h values towards the bottom half of the vane is slightly more pronounced, but generally these surfaces appear similar. While these comparisons certainly do not make any definite conclusions about vane heat transfer as a function of dilution hole placement, they do raise some questions that call for further investigation.

Chapter 5

Final Conclusions and Recommendations

Comparisons of the various configurations have brought to light two main conclusions for this research. First, reducing the distance between the dilution holes and vane leading edge by half creates high levels of uneven flow at the vane entrance and adversely effects the heat transfer levels at the vane surface. Second, the half pitch shift of the dilution holes in the span-wise direction leads to similar, if not slightly improved heat transfer effects at the vane surface and warrants further investigation.

While the distance reduction between the rows of dilution holes and first vane could serve to reduce the overall size of the combustor and in turn help to improve the power-weight ratio of an engine, the 50 percent distance reduction appears as though it would yield more problems than benefits. As shown in the results above, this distance simply does not allow the freestream flow and coolant jets enough time to mix and develop even flow at the turbine inlet. This results in larger velocity gradients at the vane and even past it, which could have detrimental effects on other downstream components. More importantly, the plots of the vane heat transfer coefficient display large variations along both the high and low pressure sides of the vane. This type of heating could enhance the effects of creep and general wear as certain areas of the vane would see more stress than other areas. It is possible that the distance between the dilution holes and first vane could be reduced, but future investigations should consider reducing this distance by less than 50 percent. If given ample time for the flows to mix and create less

dramatic velocity, pressure, and temperature gradients at the turbine inlet, this type of shift could help achieve smaller combustor sections.

The span-wise shift in the placement of dilution holes presents interesting results in the area of heat transfer. Structurally, the flow in the combustor looks very similar to the basic configuration, which was expected. However, aligning the second row of dilution holes with the vane leading edge may lead to lower and more even heat transfer at the vane surface. It may be that this alignment of the second row of holes, which are closer to the vane, presents more cooling air at the leading edge. In the basic configuration, the leading edge displays the largest values of h, which are seen to be smaller in the same regions of the periodically shifted configuration. Furthermore, the h values on the high and low pressure sides of the vane are relatively consistent with the basic configuration, if not more smooth in the center of the high pressure side. These patterns are worth delving further into to help determine if this type of shift of the dilution holes could have real advantages for the heat transfer on turbine first vanes. Additionally, if any such advantages are confirmed, combining the span-wise shift with the move of the dilution holes closer to the first vane may allow for both improved heat transfer and combustor size reduction.

Aside from these larger recommendations for future work, there are improvements that could be made in advancing this specific research. First, increasing the number of iterations on the computations, especially in the case of the span-wise shifted dilution holes, would help to verify these results. Also, increasing the quality of the grid across all the cases at the wall surfaces could help study the immediate structures created by the dilution jets as well as gain better insight about the vane-wall interfaces. Overall, this research attempted to guide more in-depth work to come, with the hope of contributing to future jet engine development.

Appendix A

Full Tables for Background/Setup

The tables and figures in this appendix provide expanded detail for the background studies completed by Vakil and Stitzel as well as further information from the setup of this modeling.

Table A-1: Coolant flow geometry and discharge coefficients from Vakil [8]

	Number of Holes	Discharge Coefficient, C_d	Diameter (cm)
Panel 1	202	0.739	0.76
Panel 2	478	0.733	0.76
Dilution Row 1	3	0.829	8.51
Panel 3	413	0.733	0.76
Dilution Row 2	2	0.912	12.12
Panel 4	130	0.739	0.76

Table A-2: Full list of boundary conditions from basic model configuration. The # column refers to number of domains incorporated in the boundary

#	Name	Type	ID
34	Connection	Connection	Connection
5	Unspecified	Unspecified	Unspecified
1	main inlet	Velocity Inlet	1
5	top wall	Wall	2
5	bottom wall	Wall	3
2	vane	Wall	4
3	front periodic	Symmetry	5
3	back periodic	Symmetry	6
12	fplen walls	Wall	7
1	ftplen inlet	Mass Flow Inlet	8
1	fbplen inlet	Mass Flow Inlet	9
16	rplen walls	Wall	10
2	rfplen periodic	Symmetry	11
2	rbplen periodic	Symmetry	12
1	rtfplen inlet	Mass Flow Inlet	13
1	rtbplen inlet	Mass Flow Inlet	14
1	rbfplen inlet	Mass Flow Inlet	15
1	rbbplen inlet	Mass Flow Inlet	16
4	fdil walls	Wall	17
4	rdil walls	Wall	18
2	rfdil periodic	Symmetry	19
2	rbdil periodic	Symmetry	20
2	main outlet	Outflow	21

Table A-3: Full set of experimental operating conditions from Vakil [8]

Atmospheric Pressure (MPa)	98.82
Freestream Temperature, T_∞ (°C)	59.04
Coolant Temperature, T_c (°C)	22.55
Freestream Density, ρ_∞ (kg/m^3)	1.00
Coolant Density, ρ_c (kg/m^3)	1.12
Fan Speed (Hz)	40.00
Inlet Velocity, u_∞ (m/s)	1.62

Table A-4: Full experimental coolant flow conditions from Vakil [8]

	% Mass Flow Addition Based on Local Flow Rate	Momentum Flux Ratio Based on Local Mass-Averaged Velocity	Mass Flux Ratio Based on Local Mass-Averaged Velocity	Density Ratio Based on Upstream Flow Conditions	Ratio of Mass-Averaged Velocity to Inlet Velocity
Panel 1	2.6	9	3.2	1.12	1
Panel 2	6.3	9	3.2	1.12	1
Panel 3	5.4	9	3.2	1.12	1.6
Panel 4	2.2	9	3.2	1.12	2.7
Dilution 1	18.5	128	12	1.12	1
Dilution 2	12.5	32	6	1.12	1.6

Appendix B

Further Computational Result Figures

This appendix includes figures from the computational models which were not included in the discussion from Chapter 4.

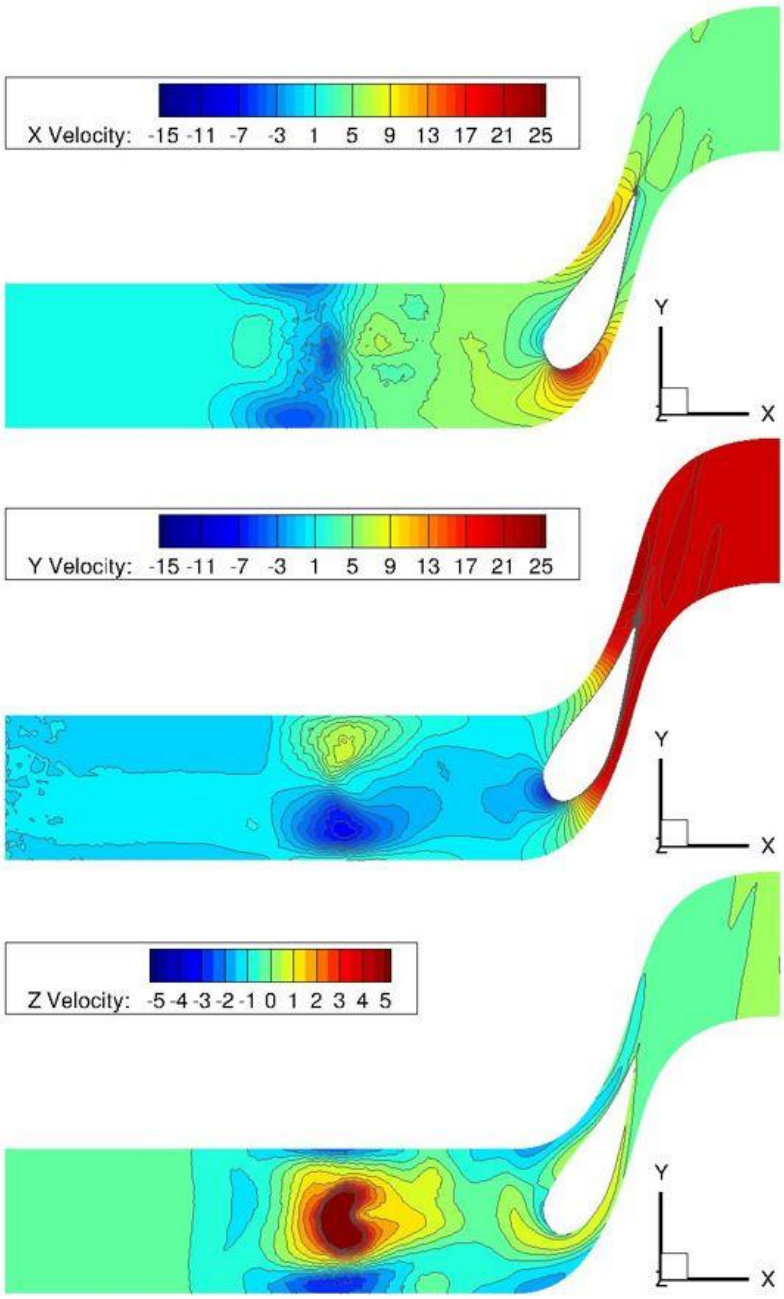

Figure B-1: Contours of velocity in m/s at midspan plane of C2

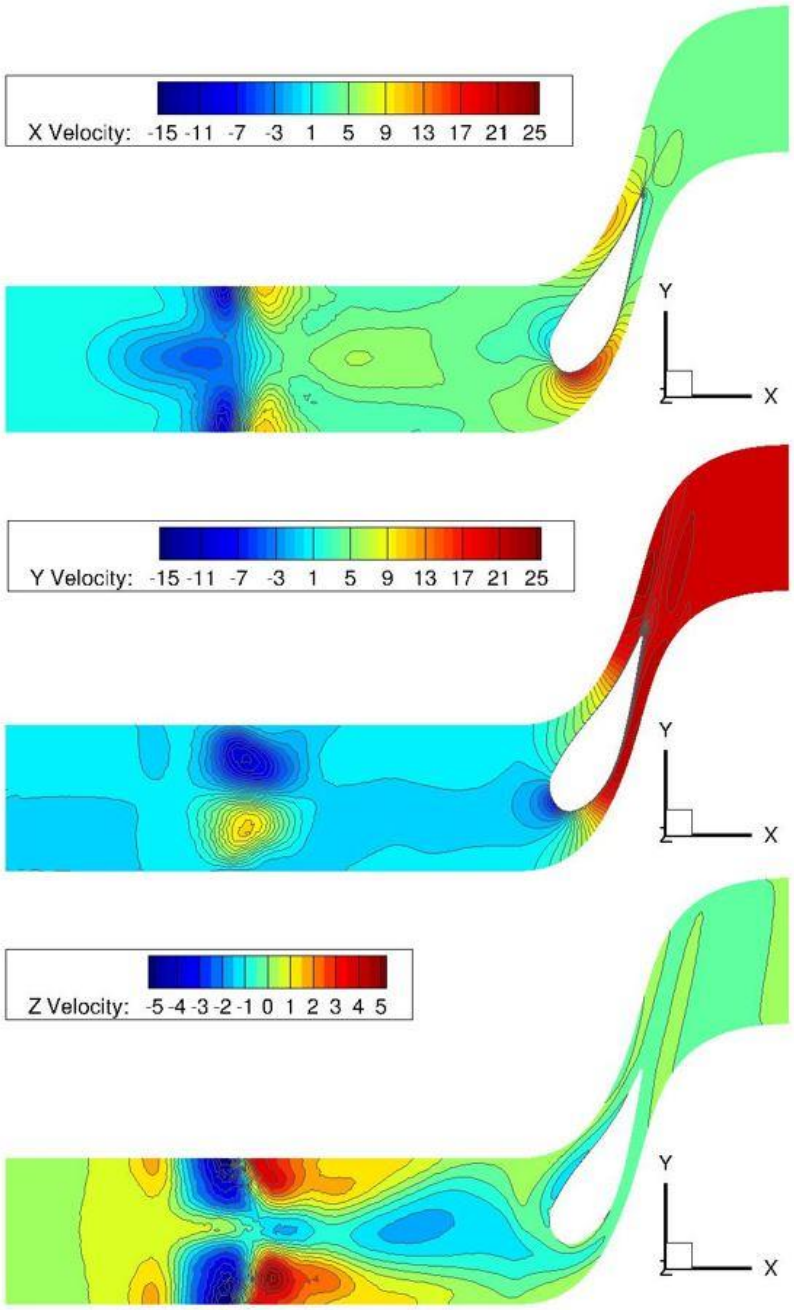

Figure B-2: Contours of velocity in m/s at midspan plane of C3

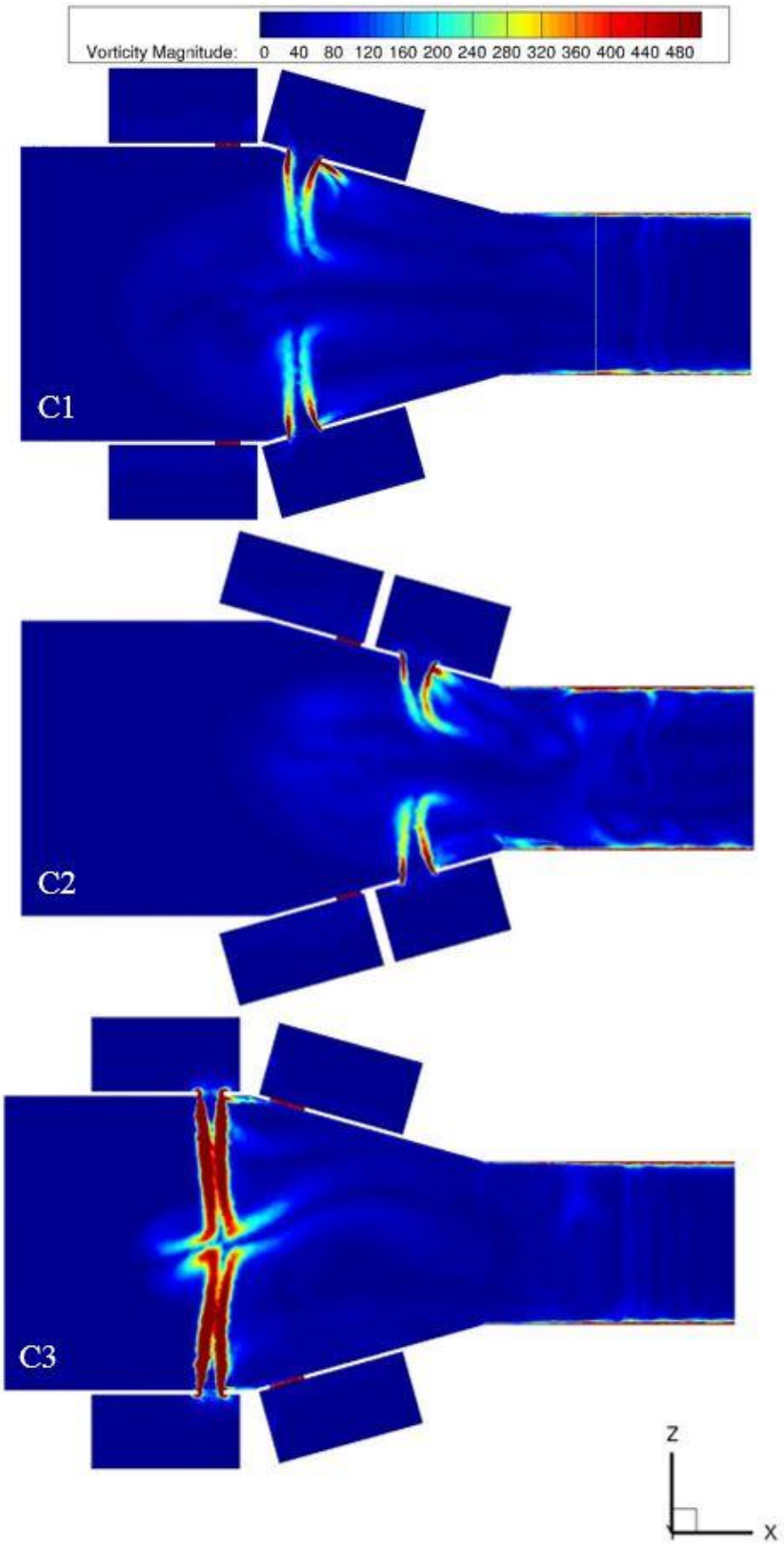

Figure B-3: Contours of vorticity on front surfaces of all configurations

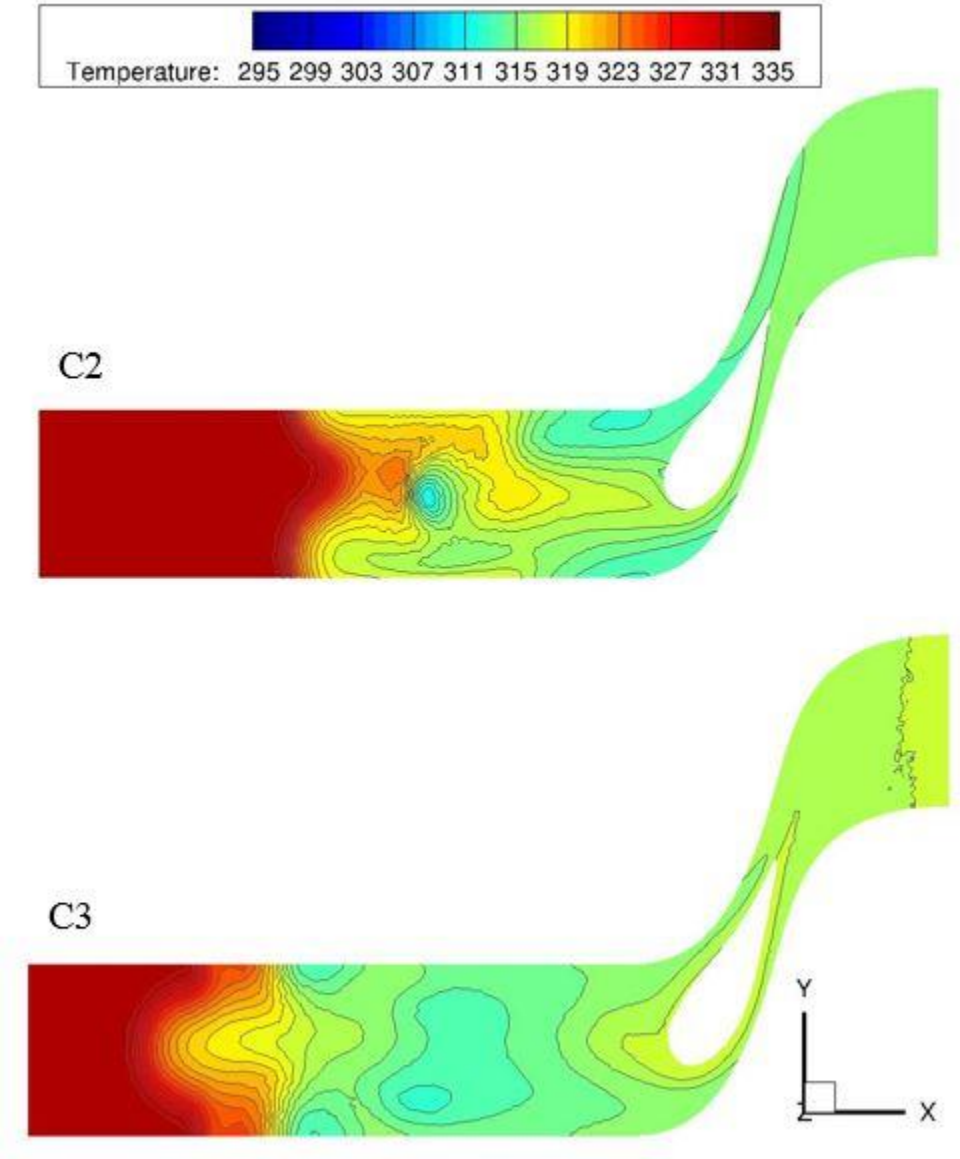

Figure B-4: Contours of temperature in K at midspan planes of C2 and C3

BIBLIOGRAPHY

1. Stitzel, S.M., *Flow Field Computations of Combustor-Turbine Interaction in a Gas Turbine Engine*, in *Mechanical Engineering*. 2001, Virginia Polytechnic Institute and State University: Blacksburg, Virginia. p. 208.
2. Horlock, J., *The basic thermodynamics of turbine cooling.* Journal of turbomachinery, 2001. **123**(3): p. 583-592.
3. Bohan, B.T. and M.D. Polanka, *Analysis of Flow Migration in an Ultra-Compact Combustor.* Journal of Engineering for Gas Turbines and Power, 2013. **135**(5): p. 051502.
4. Vakil, S.S. and K. Thole, *Flow and thermal field measurements in a combustor simulator relevant to a gas turbine aeroengine.* Journal of engineering for gas turbines and power, 2005. **127**(2): p. 257-267.
5. Scrittore, J., K. Thole, and S. Burd, *Investigation of velocity profiles for effusion cooling of a combustor liner.* Journal of turbomachinery, 2007. **129**(3): p. 518-526.
6. Rockwell, D., *Vortex-body interactions.* Annual review of fluid mechanics, 1998. **30**(1): p. 199-229.
7. Fric, T. and A. Roshko, *Vortical structure in the wake of a transverse jet.* Journal of Fluid Mechanics, 1994. **279**: p. 1-47.
8. Vakil, S.S., *Flow and Thermal Field Measurements in a Combustor Simulator Relevant to a Gas Turbine Aero-Engine* in *Mechanical Engineering*. 2002, Virginia Polytechnic Institute and State University: Blacksburg, Virginia.
9. Barringer, M., et al., *Flow field simulations of a gas turbine combustor.* Journal of Turbomachinery, 2002. **124**(3): p. 508-516.
10. Mahesh, K., et al., *Large-eddy simulation of reacting turbulent flows in complex geometries.* Journal of Applied Mechanics, 2006. **73**(3): p. 374-381.
11. Koupper, C., et al., *Development of an engine representative combustor simulator dedicated to hot streak generation.* Journal of Turbomachinery, 2014. **136**(11): p. 111007.
12. Benim, A., et al. *Analysis of Turbulent Swirling Flow in an Isothermal Gas Turbine Combustor Model*. in *ASME Turbo Expo 2014: Turbine Technical Conference and Exposition*. 2014. American Society of Mechanical Engineers.
13. Holdeman, J.D. and R. Walker, *Mixing of a Row of Jets with a Confined Crossflow.* AIAA Journal, 1977. **15**(2): p. 243-249.
14. Holdeman, J., R. Srinivasant, and A. Berenfeld, *Experiments in dilution jet mixing.* AIAA journal, 1984. **22**(10): p. 1436-1443.
15. Stevens, S. and J. Carrotte, *Experimental studies of combustor dilution zone aerodynamics. I-Mean flowfields.* Journal of Propulsion and Power, 1990. **6**(3): p. 297-304.
16. Stevens, S. and J. Carrotte, *Experimental studies of combustor dilution zone aerodynamics. II-Jet development.* Journal of Propulsion and Power, 1990. **6**(4): p. 504-511.
17. Smith, S. and M. Mungal, *Mixing, structure and scaling of the jet in crossflow.* Journal of Fluid Mechanics, 1998. **357**: p. 83-122.
18. Liscinsky, D.S., B. True, and J. Holdeman, *Experimental investigation of crossflow jet mixing in a rectangular duct*. Vol. 106152. 1993: National Aeronautics and Space Administration.
19. Holdeman, J.D., D.S. Liscinsky, and D.B. Bain, *Mixing of multiple jets with a confined subsonic crossflow: Part II—Opposed rows of orifices in rectangular ducts.* Journal of Engineering for Gas Turbines and Power, 1999. **121**(3): p. 551-562.

20. Prière, C., et al., *Experimental and numerical studies of dilution systems for low-emission combustors.* AIAA journal, 2005. **43**(8): p. 1753-1766.
21. Ames, F.E., *The influence of large-scale high-intensity turbulence on vane heat transfer.* Journal of Turbomachinery, 1997. **119**(1): p. 23-30.
22. Qureshi, I., A.D. Smith, and T. Povey, *HP vane aerodynamics and heat transfer in the presence of aggressive inlet swirl.* Journal of Turbomachinery, 2013. **135**(2): p. 021040.
23. Radomsky, R.W. and K.A. Thole, *Flowfield measurements for a highly turbulent flow in a stator vane passage.* Journal of turbomachinery, 2000. **122**(2): p. 255-262.

ACADEMIC VITA

Enrico B. Della Corna

ebd5044@psu.edu 716 C West Beaver Ave, State College, PA (412) 217-6212
8723 Woodside Court, McLean, VA

Education

The Pennsylvania State University, Schreyer Honors College — *Class of 2015*
B.S. in Mechanical Engineering, Minor in Spanish

Automotive Summer School, University Duisburg-Essen, Germany — *Summer 2013*
Attended lectures on current automotive technologies, worked alongside Phd. student involved in contact mechanics research, toured major German OEMs

Undergraduate Thesis Research — *Fall 2014-Spring 2015*
Will work to synthesize combustor and turbine design by modeling and testing the irregular flows exiting combustion chambers in jet engines

Honors
Dean's List (Awarded each semester) — *Fall 2011-Fall 2014*
National Merit Scholar Finalist/4 Year Scholarship Winner — *Fall 2011*

Work Experience

Engineering Intern at Cummins Power Generation — *Summer 2014*
Supported Mobile Consumer Products group and led improvement effort of acoustic foam sound shield for marine application generator sets in the following ways:
-Investigated foam degradation methods and genset operating conditions in the field
- Planned and coordinated acoustic performance tests to generate sound models and optimal sound shield configurations
- Joined a team to assist with cross-functional cost reduction efforts, as well as to examine the cost reduction aspect of sound shield improvement
- Ensured compliance of all sound shield components with changing industry standards through contact with suppliers and conduction of in-house flammability testing

Volunteer with Fabretto Children's Foundation — *Summer 2009-2011*
Led service trip to Nicaragua, organized service group, arranged travel, worked with Nicaraguan students, repaired entrance to Fabretto's primary distribution center

Coach at HappyFeet NOVA — *Summer 2011*
Soccer coach for children ages 2-9, led group practice sessions and coached games

Activities

Off Campus Student Union, Chair of Internal Development — *Spring 2014-Present*
Planned member events, managed alumni member relations, promoted communication between PSU students and State College residents

Homecoming Merchandising Committee, Member — *Spring 2013-Fall 2013*
Selected for committee, ran sales, organized promotional events

Intramural Sports — *Fall 2011-Present*
Soccer, Basketball, Table Tennis

Recreational Musician — *1999-Present*
Violin, Bass, Guitar

Skills

Experience with 3-D engineering drawing programs -*Solidworks, Inventor, Google SketchUp*
Experience with programming -*Matlab*
Proficiency with word processing programs -*Word, Excel, PowerPoint*
Limited working proficiency in Spanish